Flexible pivoting of the PH domain in dynamin catalyzes fission by affecting membrane properties: Insights into the molecular degrees of freedom

Kirtika Jha[1†], Krishnakanth Baratam[1†], Vikas Dubey[1], Thomas J. Pucadyil[2] and Anand Srivastava[1]*

From the [1]Molecular Biophysics Unit, Indian Institute of Science, Bangalore, Karnataka, India 560012; [2]Indian Institute of Science Education and Research, Dr. Homi Bhabha Road, Pashan, Pune, Maharashtra, India 411008

Running title: *Dynamics of the membrane-bound dynamin PHD*

† Contributed equally

* To whom correspondence should be addressed: Anand Srivastava: Molecular Biophysics Unit, Biological Sciences Division, Indian Institute of Science, Bangalore, Karnataka, India 560012; anand@iisc.ac.in; Tel. +91-80-2293-3552; Fax. +91-80-2360-0535.

Keywords: dynamin, phosphoinositide, membrane fission, molecular modelling, membrane biophysics

---

ABSTRACT

The neuronal dynamin1 functions in the release of synaptic vesicles by orchestrating a process of GTPase-dependent membrane fission. Dynamin1 associates with the plasma membrane-localized phosphatidylinositol-4,5-bisphosphate (PIP_2) through the centrally-located pleckstrin homology domain (PHD). The PHD is dispensable as fission can be managed even when the PHD-PIP_2 interaction is replaced by a generic polyhistidine- or polylysine-lipid interaction. Remarkably however, the absence of the PHD renders a dramatic dampening of the rate of fission. These observations suggest that the PHD-PIP_2 interaction could have evolved to expedite fission to fulfill the requirement of rapid kinetics of synaptic vesicle recycling. Here, we use a suite of multiscale modeling approaches that combine atomistic molecular dynamics simulations, mixed-resolution membrane mimetic models, coarse-grained molecular simulations and advanced free-energy sampling (metadynamics) methods to explore PHD-membrane interactions. Our results reveal that; (a) the binding of PHD to PIP_2-containing membranes modulates the lipids towards fission-favoring conformations and overall softens the membrane thus rendering it pliable to undergo fission, and (b) that it does so by the association of the PHD in multiple orientations using variable loops as pivots. Together, these insights provide a molecular-level understanding of the catalytic role of the PHD in dynamin-mediated membrane fission.

Dynamin is a multi-domain GTPase that self-assembles into a helical collar and catalyzes membrane fission leading to the release of nascent clathrin-coated vesicles during endocytosis (1-5). The GTPase domain (G-domain), bundle-signaling element (BSE) and the stalk domain are the three conserved domains in dynamin which are required to evoke stimulated GTPase activity upon self-assembly on the membrane (6). In addition to these domains, classical dynamins contain a proline rich domain (PRD) with which it interacts with SH3 domain-containing partner proteins and a pleckstrin-homology domain (PHD) with which it binds the plasma membrane-localized lipid phosphatidyinositol-4,5-bisphosphate (PIP_2). GTP hydrolysis is proposed to orchestrate a series of conformational changes in the self-assembly to

surmount the activation barrier to membrane fission (7,8).

Structurally, the ubiquitous dynamin1 PHD has a C-terminal α-helix and a core β-sandwich with variable loops between the β-strands that form the binding pocket for PIP_2. Crystal structure of the dynamin1 PHD (PDB: 1DYN) suggests a β-sandwich structure with two β-sheets, one with 4 and the other with 3 β-strands, oriented in an antiparallel arrangement. The structure defines 4 loops referred to as variable loops (VLs). These loops significantly differ from each other in hydrophobicity and electrostatics. VL1 (^{533}IGIMKGG^{537}) contains a hydrophobic stretch that inserts in the membrane and assists dynamin's subcellular localization (9). VL3 (**^{590}**NTEQRNVYKDY^{600}**)** is highly polar and has also been shown to be important for membrane association (10,11). While the PHD helps classical dynamins to engage with the membrane (12,13), numerous lines of evidence suggest that it functions more than a generic membrane anchor (3,14-20). Genetic neurological disorders such as centronuclear myopathies and the Charcot-Marie-Tooth disease are linked to mutations in the PHD that map to regions distinct from those involved in membrane binding (21),(22). Cellular assays combined with biochemical and microscopic analysis of membrane fission with point mutants in the PHD of dynamin1 suggest that this domain might induce local membrane curvature by shallow insertion of one of its loops (17), and that such point mutations alter dynamics and orientation of the PHD on the membrane (18). Experimentally guided modeling has shown that tilting of the PHD could be responsible for creating a low energy pathway towards reaching the hemi-fission state (23)**.** GTP hydrolysis is required to initiate fission through constriction (24) but whether this is adequate to achieve complete and leakage-free vesicle scission is still under debate (20,23,25). Recent evidence indicates that the GTPase-driven scaffold constriction brings the membrane in close proximity but not enough to cross the energy barrier for fission and that stochastic fluctuations are responsible for the crossover from the constricted stage to the hemi-fission state (20,26). Indeed, analysis of membrane fission at the single event resolution indicates that replacement of the PHD-PIP_2 interaction with a generic lipid-protein interaction forms long-lived, highly constricted pre-fission intermediates on the membrane which manifests in a dramatic dampening of fission kinetics (3). Recent cryo-EM data of the dynamin polymer assembled on tubular membranes reveal complex and variable geometries of the PHD. The variable PHD configurations may reflect an evolutionary requirement for traversing a pathway whereby membrane constriction guarantees leakage-free fission (23,25,27,28).

Guided by these observations, and since short-lived transitions states reflecting an evolving PHD-PIP_2 interaction within the scaffold are difficult to capture experimentally, we described results from molecular dynamics simulations of the PHD on a PIP_2-containing membrane. Using multi-scale molecular simulations, we first analyze the undulation spectra of large membrane system with and without the PHD to analyze the effect on membrane physical properties. Together, these methods also test the hypothesis of local curvature generation by the PHD. Next, we analyze membrane association geometries of the PHD using various methods involving both all-atom (AA) and coarse-grained (CG) molecular dynamics simulations as well as free energy calculations using enhanced sampling methods. We extend this analysis by performing mixed-resolution Highly Mobile Membrane-Mimetic Model (HMMM)-based molecular dynamics simulations (31) with the PHD on the membrane under different initial orientations to explore possible membrane association pathways. Together, our results indicate that the presence of the PHD causes significant changes in lipid conformations and the membrane bending rigidity thus providing mechanistic insights into its catalytic effect on membrane fission. These effects are managed by flexible pivoting of the previously described variable loop1 (VL1) and a novel fourth variable loop (VL4) in the PHD with the membrane.

Results

Binding of the PHD renders the membrane pliable for fission

To determine the effect of the PHD on the physical properties of the membrane, we performed coarse-grained (CG) simulations using the Martini force field of a large (~625 nm^2) bilayer patch. The bilayer is comprised of 2048 lipids with DOPC:DOPS:PIP_2 in 80:19:1 molar ratio. On to this bilayer, 14 CG PHD

units were mounted randomly on one of the leaflets. Simulations were performed for 4 μs. The bending moduli data from undulation spectra fitted to regular Helfrich theory is provided in Table 1 and the calculations show that the presence of the PHDs reduces the bending modulus of the lipid (Table 1). Thus, the bending modulus (K_c) of the membrane with PHDs is about 8 k_BT lower than without, signifying that the PHDs increase the natural thermal undulations in the membrane. To further quantitate these effects, we analyzed trajectories by fitting the spectra to a modified Helfrich formulation wherein the curvature and undulations are coupled (29). This was done because soft lipid bilayers have scale-rich undulations that can be difficult to distinguish from the long wavelengths and curvature field fluctuations induced by proteins. The Hamiltonian with the curvature coupling used to fit the spectra is shown in equation 1 below (32).

$$\mathcal{H} = A\sum_{q}\left\{\langle|h_q|^2\rangle\left(\frac{1}{2}k_c q^4 + \frac{1}{2}\gamma q^2\right) + \left(k_c\left\{\langle h_q C_{0,q}\rangle q^2 + \langle C_{0,q}{}^2\rangle\right)\right\}\right\} \quad (1)$$

We applied this formulation to two systems, one where the PHDs are randomly distributed on the membrane (Fig. 1A), and the other where the PHDs are arranged contiguously on the membrane (Fig. 1B). The latter was performed to mimic the organization of the PHDs in a self-assembled dynamin collar. The fit to the spectra to Equation 1 is shown in Fig. 1C and the curvature profile is shown in Fig. 1D. The curvature field is not significant and does not have a noticeable change in the modulus (~1-2 k_BT) as compared to data in Table 1 for the WT systems. Together these results confirm that PHDs soften the bilayer irrespective of the manner in which they are organized on the membrane. The implication of this "softening" of the membrane in terms of the two paradigmatic models of membrane fission, namely the "*instability model*" (30,31) and the "*catalytic model*" (23,32) are discussed in detail later in the text.

Based on our finding that the presence of the PHD lowers the bending modulus of the membrane, we focused on the molecular structure of lipids such as their tilt and splay since these have been reported to influence membrane fission (32). To get insights into the molecular structures and changes related to the two-dimensional density structure factor of the membrane, we first plotted the full height undulation spectra (see Fig. S1 in SI) with larger q-regimes. In this completely Fourier-based approach to the calculations of the fluctuation spectrum, we did not see any remarkable signature of a protrusion regime when interpreting the spectra (33). It has been discussed earlier (34,35) that the simulated spectra outside of the low q-limit (wavelengths larger than membrane thickness) should be interpreted in terms of tilting (and splaying) behavior. For this, we generated a microsecond-long atomistic trajectory of a single PHD on a lipid bilayer composed of DOPC: DOPS: PIP_2 (80:19:1) and analyzed effects on membrane thickness and lipid conformations (tilt and splay) in areas proximal and distal to the PHD on the membrane. Fig. 2A shows a snapshot of the bilayer-PHD system with the proximal and distal lipids marked in different colors. Fig 2B shows the variation of membrane thickness across the cross-section of the bilayer averaged over a 250 ns-long time period. Remarkably, the PHD influences the underlying membrane by thinning it by around 0.4 nm (Fig. 2B). Similar analyses for different 250 ns-long time-averaged plots show that membrane thinning is tightly coupled to the location of the PHD (Fig. S2, top panel). Indeed, presence of the PHD leads to a positive lipid splay in proximal lipids (36) and is seen by measurements of the lipid tail (Fig. 2C) and head (Fig. 2D) tilt angles for a 25 ns time period. Lipid tail tilt is defined by the angle between the membrane normal and the vector formed by the glycerol carbon and the last tail atom. Lipid head tilt is defined by the angle between P-N vector (vector formed by Phosphorus and Nitrogen atom in the lipid) and the membrane normal. As seen in Figs. 2C and 2D, presence of the PHD induces significant fluctuations in the tail and head tilt angles in lipids proximal to the PHD than in the distal lipids or in lipids in a membrane without the PHD. Snapshots of tilt and splay for a proximal and distal lipid are shown in Fig. S2 and highlight the extent to which the PHD influences local lipid dynamics. That the PHD can cause such remarkable changes in tilt fluctuations of lipids strongly suggests the possibility that its engagement with the membrane could prime proximal lipids to attain non-bilayer intermediates and thereby lower the energy barrier for fission. Importantly, the significant changes seen in the tilt values and the higher populations of tilt angles from the

average emphasize the need to go beyond the simple Helfrich model, including those with undulation-curvature coupling, to understand energetics of membrane remodeling in terms of finer degrees of freedom such as tilt and splay modulus (32,37).

We also carried out additional undulation spectra analysis with trajectories that were generated using certain "fission-inhibiting" mutations on the PHDs. Those results are discussed later since the choice of the mutations was made based on the HMMM simulations and metadynamics-based free-energy calculations that is covered later in the paper.

PHDs can associate with membrane in multiple orientations

Recent cryoEM reconstructions of the dynamin polymer assembled on a membrane report of a super-constricted state at 10.1 Å resolution, which highlights localized conformational changes at the BSE and GTPase domains that drive membrane constriction on GTP hydrolysis. Reconstructing this data and focusing on the PHD orientation by taking slices across the collar revealed interesting results (Fig. 3A). PHD orientation about a ring of the dynamin polymer was measured by plotting the distribution of the angle between the major inertial axis of each PHD and the vector that connects the center of the ring with the centroid of the PHD (Fig. 3B, see inset in Fig. 3A for a schematic of the angle measurement for a single slice). This analysis revealed that the membrane-bound PHDs adopt a wide range of orientations in the polymer. This is also apparent in other slices analyzed in the polymer (Fig. S3). The wide range of PHD orientations, even in the highly packed constricted state of the dynamin polymer, suggests that the PHD has the inherent ability to associate with the membrane in multiple orientations.

To test this, we carried out advanced mixed-resolution molecular simulations using the highly mobile membrane-mimetic model (HMMM) (38-40). HMMM simulations provide insights into the molecular-level association between the PHD and the lipid bilayer. This model utilizes a biphasic setup comprising of lipids with short-chain fatty acyl chains (typically 3-5 carbon atoms-long) organized around an organic solvent, 1,1-dichloro-ethane (DCLE), which mimics the hydrophobic core of the membrane. The HMMM model is ideal for studying membrane-associated phenomena through MD simulations without compromising on the atomic details of the protein-lipid headgroup interface since lipid diffusion in the bilayer is accelerated by an order of magnitude due to the absence of tail friction (41-43). We ran 8 different HMMM simulations with different initial orientations of the PHD on a bilayer composed of PC:PS:PIP_2 (80:19:1 mol%) and a DCLE hydrophobic core. Six systems had the initial orientation of the different variable loops close to PIP_2 in the membrane while 2 had the PHD placed in an inverted initial orientation (see Table 2). Each simulation was evolved for a minimum of 100 ns. Two important observations stand out from these simulations. Firstly, despite drastically different initial orientations, the system evolves showing that VL1 (^{531}IGIMKGG) and VL4 (^{577}KGFMSSK) and to some extent VL3 (^{590}NTEQRNVYKDY) partition into the membrane. Figure 4 shows the initial and final orientations as well as the z-distance of specific loop residues in the PHD from the phosphate plane of the membrane. See Fig. S4 for data on other systems. Results on VL1 are consistent with previous studies indicating that it acts as an anchor in the membrane (14,15,44,45). Indeed, the I533A mutation is known to destabilize this interaction and reduced the stability of the scaffold on the membrane in the wake of GTP hydrolysis (3,17). The role of VL3 in stable phosphoinositide binding has also been shown earlier (6,16,18,46) and the Y600L mutation impairs membrane fission in vitro (11). However, a plot of the z-distance of the C-alpha and z-distance of the terminal 'hydroxyl oxygen' atom of Y600 as a function of time reveals marginal association with the membrane (Fig S5). The association however is deeper if considered from the side chain depth profile (Fig. S5). In the movie file (movie1) that depicts a quintessential HMMM run, we show the dynamics of the association of the PHD with the membrane. The VL1, VL3 and VL4 loops are marked as blue, red and orange in color, respectively and the PHD is initially oriented such that loops are facing away from the membrane. To our surprise, VL4 loop shows highly stable membrane association and this observation is consistent across different starting configurations. We further validate this observation through metadynamics advanced-sampling simulations (see below) that

remarkably shows that pockets formed by VL1-VL3 and VL1-VL4 are both available for binding the inositol headgroup. The second clear observation from our HMMM runs is that the PHD can adopt multiple orientations, despite being hinged to the membrane with any of the three VLs, which suggests that it acts more like a shallow pivot than a deep wedge or a cantilever. The degeneracy in binding (also shown through metadynamics simulations, see below) allows the PHD to bind the membrane in various geometries with the VL1 acting as a permanent anchor and the VL3 or VL4 acting as a secondary anchor that together coordinate the phosphoinositide binding.

Key residues stabilizing the PIP2-PHD binding are found in multiple VLs

We carried out "plain" metadynamics simulations (47) to obtain the docking geometry and the free-energy of docking of the PHD with IP_3 as a headgroup mimic of the $PI(4,5)P_2$ lipid. This method recapitulates real dynamics of the headgroup entering and exiting the binding pocket in the PHD and in doing so reconstructs the free energy landscape of the process. We also supplement the plain metadynamics simulations with advanced well-tempered metadynamics simulation (48-51) to get deeper insights into the variety of binding stereochemistry that seem to populate the basin around the free energy minima. Plain metadynamics simulations assume knowledge of the docking site and the method computes $\Delta\Delta G$ of the docked and free ligand states. Plain metadynamics simulations were run on two systems. The first and second assume the pocket between VL1-VL3 and between VL1-VL4 to represent the putative binding, respectively. Fig. 5 (top panel) shows how the metadynamics collective variables (CVs) are defined for the two systems and Fig. S6 shows the evolution of the ligand-protein distance as a function of the total simulation time for the two systems. CV can be thought of as reaction coordinates or order parameters that can distinguish between different conformational states of the PIP_2-PHD complex in this work. The free energy surface (FES) is calculated at the time when the IP_3 ligand crosses over from solution to the pocket and back to solution (shown as a red arrow marked "re-crossing"). The FES is shown in Fig. 5 (A2) and Fig 5 (B2) for the two systems, respectively and the lowest energy binding poses for the two systems are shown as Ligplot in Fig. 5(A3) and Fig. 5(B3), respectively. For the first system, 2D-representation of binding sites indicates that the complex is stabilized by K^{535} in VL1 and D^{599} in VL3. For the second system, I^{533} and S^{538} in VL1 and K^{583} in VL4 are the important stabilizing residues. The free energy barriers, shown by the FES profiles, are equivalent for two systems thus suggesting that both pockets bind the ligand with equal probabilities

To extend these results, we carried out well tempered-metadynamics simulations on three different systems; two where the distance CVs are chosen such that the variable loops are sampled preferentially and another with no bias for any loop or pocket. The schematics of CV selection is shown in Fig. 6 (left column) and the corresponding FES profiles are shown in right panel. The details of CV definition is discussed elsewhere. The results validate our earlier observations about different residues from different VLs capable of stabilizing the membrane association interactions**.** The convergence plot for the three systems and the time evolution of distance in and out of the ligand from domain's pocket is show in Fig. S7. In order to explore if a variety of binding geometries exist, we considered the geometries in the range of ~$2k_BT$ of the deepest minimum. We observe a range of possible geometries (Fig 7), which suggest degeneracy implying that PIP_2 can bind with different sets of residues in the PHD.

After successfully obtaining the binding poses from the metadynamics simulations and exploring different orientations from HMMM simulations, we performed a series of atomistics molecular dynamics simulations with WT and mutated PHD to further scrutinize the role of VLs, with specific focus on residues critical for membrane association. We used 3 different lipid compositions (80:20 DOPC-DOPS, 80:19:1 DOPC-DOPS-PIP2 and 60:40 DOPC-DOPS). We picked a few residues for mutations from the list obtained from HMMM and metadyanmics studies. The different membrane composition and mutants that were tested are listed in Table 3. Simulation outputs were analyzed by a simple Z-distance calculation between the $C\alpha$ atoms of each residue with the z-coordinate of the phosphate plane of the bilayer. As shown in Fig. 8A, the I533A mutation in VL1 severely affects membrane association with the entire domain moving

away from the membrane. This is consistent with the dramatically reduced fission efficiency seen in reconstitution studies with this mutant earlier (3,17). Figs. 8B, C show the effects of F579A in VL4 as well as K539A;K583A mutations in VL1 and VL4, respectively. To understand the membrane association mechanism of F^{579} this residue was mutated to a positively charged lysine residue or to a hydrophobic tryptophan residue and tested on membranes of different compositions. The results are shown in Fig. S8 with observations and analysis. Besides the double mutations (K539A+K583A), independent single mutations were also done for K539 and K583. The results are shown in Fig. S9. The F579 and K583A mutations are mildly disrupting the membrane association and interestingly the effect is more pronounced in the VL1 regions. We also tried Y600L and Y600A mutations but did not see any remarkable changes in membrane association (data not shown). The height fluctuations evolution of each residue from the membrane for F579A, K539A, K583A and K593A-K583A are shown as movie files in SI.

Discussion

The dynamin collar undergoes a series of segmental rearrangements while executing membrane fission. Each PHD must be capable of adapting to be the progressively remodeled underlying membrane. Previous results from 3D reconstructions of dynamin mutants trapped in a constricted state (27,28,52) as well as from biochemical and multiple fluorescence spectroscopic and microscopic approaches (18) suggest that the PHD can associate with the membrane in different orientations. Theoretical analyses of determinants that could lower the energy barrier for fission have invoked tilting of the PHD to conform with the evolving membrane curvature and thereby create a low-energy pathway for hemi-fission (23). Our results on a comprehensive molecular dynamics simulation validate these possibilities. Fundamentally, binding of the PHDs lowers the membrane rigidity. This effect is attributed to specific binding since PHD mutants that display reduced membrane association fail to elicit this effect. Thus, the membrane bending moduli seen with I533A, F579A and the double mutant K539A+K583A are higher by 2-5 k_BT than seen with WT (Table 1), indicating that specific molecular interactions confer a global change in the bulk physical properties of the membrane.

Recent evidence of the existence of non-bilayer configurations of lipids formed at the stalk and hemi-fission intermediates (53-57) prompted us to go beyond models that assume the membrane as an elastic sheet capable of undergoing fission through curvature instability (11,30,58-60) and focus on the molecular degrees of freedom of constituent lipids. Thus, higher fluctuations in the lipid tilt and splay may have a significant role in facilitating the membrane to stochastically crossover to the non-bilayer intermediates once a threshold constriction of the lumen is reached. The formation of non-bilayer intermediates dictates that a physical coupling between the two leaflets of the bilayer is reduced (61). However, our analysis reveals no apparent change in the interdigitation between the two leaflets and this could reflect the fact that our simulations are currently not designed to recapitulate dynamics of the constricted tubular intermediate see during fission.

The PHD is a ubiquitous membrane-binding domain. Several studies have explored the molecular mechanism by which it associates with PIP_2 in the membrane (62-68). Analysis of inositol-bound PHD structures clearly reveal the presence of a highly basic region that favors binding to the highly anionic phosphoinositide lipids (69,70). Our results extend these models and provide a molecular-level explanation for how it engages with PIP_2 in the membrane. Thus, molecular simulations where the PHDs is placed inverted on the membrane result in its reorientation and specific association of the VL loops with the membrane (movie1). Furthermore, together with results from HMMM, we identify novel interactions between VL4 and the membrane, which we believe is a significant finding that needs experimental validation. Remarkably, although the PHDs display specificity towards PIP_2, the binding per se is degenerate such the PIP_2-engaged PHD adopts multiple orientations. Given that the membrane is a heterogeneous ensemble of multiple fluctuating states, this degeneracy could facilitate recognition of such heterogeneity on the membrane surface. In this regard, previous models on conditionality of binding of peripheral membrane proteins could be understood within a framework of recognition of such heterogeneity rather than as a single

binding event of a domain to a well-defined ligand.

Despite the fact that all three VLs appear to engage with the membrane, albeit to different extents, the degeneracy in orientations lend credence to the notion that unlike being rigidly clamped to the membrane or act as a wedge, the PHD are best represented as units that are flexible and elastically pinned to the membrane. Thus, together, our results indicate the PHDs to be flexible pivots that act to catalyze membrane fission by affecting membrane physical properties.

Material and Methods

Coarse-grained Simulations: Coarse-grained simulations were performed using GROMACS (Version 5.1.2) with MARTINI Polarizable force-field (Version 2.2P) (71-73). Lipid membranes were generated using CHARMM-GUI online server (74). Identical lipid compositions with DOPC-DOPS-PIP2 (80-19-1 %) was used for all the systems that were taken into consideration: (a) 2048 lipids pure lipid bilayer (b) 2048 lipids with 14 dyn1-PHDs (WT) (c) 2048 lipids with 14 dyn1-PHDs (I533A) (d) 2048 lipids with 14 dyn1-PHDs (F579A) (e) 2048 lipids with 14 dyn1-PHDs (K539A and K583A) simulations performed for 2 microseconds at T=310K and 1 atm pressure. Systems were minimized using steepest descent algorithm followed by the equilibration of 5-10ns. Temperature was coupled using V-rescale thermostat. Pressure coupling was performed using Berendsen barostat using semi-isotropic coupling scheme. To characterize role of dyn1-PHD in dynamin mediated fission especially how it affects the mechanistic properties of the lipid bilayer fluctuation spectra was extracted from each coarse-grained simulation. Furthermore, an estimated value of bending-modulus was obtained fitting the data using the curvature-undulation corrected Helfrich theory as shown in equation 1 (29,33).

HMMM Simulations: HMMM simulations were performed on eight systems (Table 2), each with a different initial orientation of dyn1-PHD mounted on the membrane (38). The membrane was composed of 80:19:1 mixture of DOPC, DOPS and POPI headgroups (100 lipid molecules per leaflet). The core of the bilayer was made of DCLE molecules (~1200). The bilayer-PHD systems were solvated with water molecules and Sodium and Chloride ions were added to neutralize each system and bring the salt concentration to 150 mM using VMD (75). For each system, the following simulation protocol was used: the system was equilibrated for 10 ns prior to a NVT simulation of 100 ns. Each system is simulated using NAMD 2.12 (76) with CHARMM36m protein force field (77) and the CHARMM36 lipid force field (78) with a 2 fs time step. Non-bonded forces were calculated with a 12 Å cutoff (10 Å switching distance). Long-range electrostatic forces were calculated every other time step using the particle mesh Ewald method (79). The system is maintained at a temperature of 310 K using Langevin thermostat with friction coefficient of 0.5 ps^{-1}. The choice of the initial systems were guided by inputs from Orientations of proteins in membranes (OPM) database (80).

All-Atom Simulations: A series of NPT-simulations were performed using NAMD (Version 2.11) for 100 ns with 3 different lipid membrane compositions to understand the dynamics of dyn1-PHD in the presence of certain mutations on membrane surface (Table 4). Systems were initially minimized and followed by equilibration of 5-10 ns. Each system comprised of PHD, 200 lipids, ~23000 water molecules and 0.15 NaCl. As previously, CHARMM36 force-field (78) was used for particle definitions. To carry out the analysis of thickness variation across the membrane surface, interdigitation and lipid tilt and splay fluctuation, either in-house VMD TCL script were used or the VMD membrane plugin tool (81) was used.

Cryo-EM Images: Cryo-EM map (28) for the constricted collar (K44A mutant) of dynamin (EMD-2701) is obtained from EM databank (www.emdatabank.org). The map is visualized using chimera (82) and is colored according to the cylinder radius.

Metadynamics: The X-ray solved structure of dyn1-PHD was obtained from protein data bank (1DYN) (83). The force-field parameters of ligand corresponding toCHARMM22 force-field were generated using swissparam server (84). The initial configurations of the protein-ligand system were constructed in cubic box using PYMOL (85). The systems were then solvated with TIP3P water molecules and

neutralized using 0.15 M NaCl. All the systems were energy minimized and equilibrated to a temperature of 310 K and 1 atm pressure before proceeding to production runs. Velocity rescaling algorithm (86) with (time constant of 0.1 ps) and Parrinello-Rahman algorithm for (87) (time constant of 2 ps) were used to maintain temperature and pressure, respectively. Bond constraints were dealt using LINCS algorithm (88). The long-range electrostatic interactions were dealt using particle mesh Ewald scheme with order 4 and a Fourier spacing of 0.16 while the short-range interactions were dealt using Verlet scheme with a cutoff of 1.4 nm. All the simulations were performed in GROMACS-5.1.4 (89) patched with PLUMED-2.3.5 (90). Production runs of 10 ns were performed before proceeding for metadynamics runs. The details of different systems and their respective collective variables can be found in SI.

Acknowledgements: AS would like to thank Dr. Ryan Bradley from Prof. Ravi Radhakrishnan's lab for his help in the analysis and interpretations of the curvature-undulation coupling of the membrane fluctuation spectra. KJ and AS would like to thank Shashank Pant for his help in teaching us how to setup and run HMMM simulations. AS would also like to thank Prof. Raghavan Varadarajan for carefully reading the manuscript and for his comments.

Conflict of interest: The authors declare that they have no conflicts of interest with the contents of this article.

Author contributions: TJP and AS conceived the idea and designed the experiments. KJ performed and analysed the HMMM simulations. KJ and KB processed the recently published cryo-EM electron density map for dynamin collar on the membrane, reconstructed and analysed the images. KB carried out the plain and well-tempered metadynamics simulations and analysed the data. VD and AS setup and ran the large scale CGMD Martini simulations and AAMD simulations and analysed the data. AS wrote the paper with help of all co-authors.

References

1. Faelber, K., Posor, Y., Gao, S., Held, M., Roske, Y., Schulze, D., Haucke, V., Noé, F., and Daumke, O. (2011) Crystal structure of nucleotide-free dynamin. *Nature* **477**, 556
2. Morlot, S., and Roux, A. (2013) Mechanics of dynamin-mediated membrane fission. *Annual review of biophysics* **42**, 629-649
3. Dar, S., and Pucadyil, T. J. (2017) The pleckstrin-homology domain of dynamin is dispensable for membrane constriction and fission. *Molecular biology of the cell* **28**, 152-160
4. Koenig, J., Saito, K., and Ikeda, K. (1983) Reversible control of synaptic transmission in a single gene mutant of Drosophila melanogaster. *The Journal of cell biology* **96**, 1517-1522
5. van der Bliek, A. M., Redelmeier, T. E., Damke, H., Tisdale, E. J., Meyerowitz, E. M., and Schmid, S. L. (1993) Mutations in human dynamin block an intermediate stage in coated vesicle formation. *The Journal of cell biology* **122**, 553-563
6. Chappie, J. S., and Dyda, F. (2013) Building a fission machine–structural insights into dynamin assembly and activation. *J Cell Sci*, jcs. 108845
7. Schneck, E., Sedlmeier, F., and Netz, R. R. (2012) Hydration repulsion between biomembranes results from an interplay of dehydration and depolarization. *Proceedings of the National Academy of Sciences* **109**, 14405-14409
8. Chernomordik, L. V., and Kozlov, M. M. (2003) Protein-lipid interplay in fusion and fission of biological membranes. *Annual review of biochemistry* **72**, 175-207
9. Ramachandran, R., Surka, M., Chappie, J. S., Fowler, D. M., Foss, T. R., Song, B. D., and Schmid, S. L. (2007) The dynamin middle domain is critical for tetramerization and higher-order self-assembly. *The EMBO journal* **26**, 559-566
10. Francy, C. A., Alvarez, F. J., Zhou, L., Ramachandran, R., and Mears, J. A. (2015) The mechanoenzymatic core of dynamin-related protein 1 comprises the minimal machinery required for membrane constriction. *Journal of Biological Chemistry*, jbc. M114. 610881
11. Liu, Y.-W., Neumann, S., Ramachandran, R., Ferguson, S. M., Pucadyil, T. J., and Schmid, S. L. (2011) Differential curvature sensing and generating activities of dynamin isoforms provide opportunities for tissue-specific regulation. *Proceedings of the National Academy of Sciences* **108**, E234-E242
12. Okamoto, P. M., Herskovits, J. S., and Vallee, R. B. (1997) Role of the basic, proline-rich region of dynamin in Src homology 3 domain binding and endocytosis. *Journal of Biological Chemistry* **272**, 11629-11635
13. Ferguson, S. M., and De Camilli, P. (2012) Dynamin, a membrane-remodelling GTPase. *Nature reviews Molecular cell biology* **13**, 75
14. Klein, D. E., Lee, A., Frank, D. W., Marks, M. S., and Lemmon, M. A. (1998) The pleckstrin homology domains of dynamin isoforms require oligomerization for high affinity phosphoinositide binding. *Journal of Biological Chemistry* **273**, 27725-27733
15. Achiriloaie, M., Barylko, B., and Albanesi, J. P. (1999) Essential role of the dynamin pleckstrin homology domain in receptor-mediated endocytosis. *Molecular and Cellular Biology* **19**, 1410-1415
16. Vallis, Y., Wigge, P., Marks, B., Evans, P. R., and McMahon, H. T. (1999) Importance of the pleckstrin homology domain of dynamin in clathrin-mediated endocytosis. *Current biology* **9**, 257-263
17. Ramachandran, R., Pucadyil, T. J., Liu, Y.-W., Acharya, S., Leonard, M., Lukiyanchuk, V., and Schmid, S. L. (2009) Membrane insertion of the pleckstrin homology domain variable loop 1 is critical for dynamin-catalyzed vesicle scission. *Molecular biology of the cell* **20**, 4630-4639
18. Mehrotra, N., Nichols, J., and Ramachandran, R. (2014) Alternate pleckstrin homology domain orientations regulate dynamin-catalyzed membrane fission. *Molecular biology of the cell* **25**, 879-890
19. Reubold, T. F., Faelber, K., Plattner, N., Posor, Y., Ketel, K., Curth, U., Schlegel, J., Anand, R., Manstein, D. J., and Noé, F. (2015) Crystal structure of the dynamin tetramer. *Nature* **525**, 404
20. Terzi, M. M., and Deserno, M. (2016) Revisiting Tilt in Classical Curvature Elastic Theories for Membranes. *Biophysical Journal* **110**, 581a

21. Durieux, A.-C., Prudhon, B., Guicheney, P., and Bitoun, M. (2010) Dynamin 2 and human diseases. *Journal of molecular medicine* **88**, 339-350
22. Kenniston, J. A., and Lemmon, M. A. (2010) Dynamin GTPase regulation is altered by PH domain mutations found in centronuclear myopathy patients. *The EMBO journal* **29**, 3054-3067
23. Shnyrova, A. V., Bashkirov, P. V., Akimov, S. A., Pucadyil, T. J., Zimmerberg, J., Schmid, S. L., and Frolov, V. A. (2013) Geometric catalysis of membrane fission driven by flexible dynamin rings. *Science* **339**, 1433-1436
24. Antonny, B., Burd, C., De Camilli, P., Chen, E., Daumke, O., Faelber, K., Ford, M., Frolov, V. A., Frost, A., and Hinshaw, J. E. (2016) Membrane fission by dynamin: what we know and what we need to know. *The EMBO journal* **35**, 2270-2284
25. Mattila, J.-P., Shnyrova, A. V., Sundborger, A. C., Hortelano, E. R., Fuhrmans, M., Neumann, S., Müller, M., Hinshaw, J. E., Schmid, S. L., and Frolov, V. A. (2015) A hemi-fission intermediate links two mechanistically distinct stages of membrane fission. *Nature* **524**, 109
26. Bassereau, P., Jin, R., Baumgart, T., Deserno, M., Dimova, R., Frolov, V. A., Bashkirov, P. V., Grubmüller, H., Jahn, R., and Risselada, H. J. (2018) The 2018 biomembrane curvature and remodeling roadmap. *Journal of Physics D: Applied Physics* **51**, 343001
27. Sundborger, A. C., Fang, S., Heymann, J. A., Ray, P., Chappie, J. S., and Hinshaw, J. E. (2014) A dynamin mutant defines a superconstricted prefission state. *Cell Reports* **8**, 734-742
28. Kong, L., Sochacki, K. A., Wang, H., Fang, S., Canagarajah, B., Kehr, A. D., Rice, W. J., Strub, M.-P., Taraska, J. W., and Hinshaw, J. E. (2018) Cryo-EM of the dynamin polymer assembled on lipid membrane. *Nature* **560**, 258
29. Bradley, R. P., and Radhakrishnan, R. (2016) Curvature–undulation coupling as a basis for curvature sensing and generation in bilayer membranes. *Proceedings of the National Academy of Sciences* **113**, E5117-E5124
30. Leibler, S. (1986) Curvature instability in membranes. *Journal de Physique* **47**, 507-516
31. Shlomovitz, R., Gov, N., and Roux, A. (2011) Membrane-mediated interactions and the dynamics of dynamin oligomers on membrane tubes. *New Journal of Physics* **13**, 065008
32. McDargh, Z. A., and Deserno, M. (2018) Dynamin's helical geometry does not destabilize membranes during fission. *Traffic* **19**, 328-335
33. Brandt, E. G., Braun, A. R., Sachs, J. N., Nagle, J. F., and Edholm, O. (2011) Interpretation of fluctuation spectra in lipid bilayer simulations. *Biophysical journal* **100**, 2104-2111
34. Watson, M. C., Penev, E. S., Welch, P. M., and Brown, F. L. (2011) Thermal fluctuations in shape, thickness, and molecular orientation in lipid bilayers. *The Journal of chemical physics* **135**, 244701
35. Hamm, M., and Kozlov, M. (2000) Elastic energy of tilt and bending of fluid membranes. *The European Physical Journal E* **3**, 323-335
36. Agrawal, H., Zelisko, M., Liu, L., and Sharma, P. (2016) Rigid proteins and softening of biological membranes—with application to HIV-induced cell membrane softening. *Scientific Reports* **6**, 25412
37. Nagle, J. F. (2017) Experimentally determined tilt and bending moduli of single-component lipid bilayers. *Chemistry and physics of lipids* **205**, 18-24
38. Vermaas, J. V., and Tajkhorshid, E. (2013) A microscopic view of phospholipid insertion into biological membranes. *The Journal of Physical Chemistry B* **118**, 1754-1764
39. Tajkhorshid, E. (2012) Accelerating Membrane Insertion of Peripheral Proteins with a Novel Membrane Mimetic Model. *Biophysical Journal* **102**, 6a
40. Baylon, J. L., Vermaas, J. V., Muller, M. P., Arcario, M. J., Pogorelov, T. V., and Tajkhorshid, E. (2016) Atomic-level description of protein–lipid interactions using an accelerated membrane model. *Biochimica et Biophysica Acta (BBA)-Biomembranes* **1858**, 1573-1583
41. Baylon, J. L., Lenov, I. L., Sligar, S. G., and Tajkhorshid, E. (2013) Characterizing the membrane-bound state of cytochrome P450 3A4: structure, depth of insertion, and orientation. *Journal of the American Chemical Society* **135**, 8542-8551

42. Blanchard, A. E., Arcario, M. J., Schulten, K., and Tajkhorshid, E. (2014) A highly tilted membrane configuration for the prefusion state of synaptobrevin. *Biophysical journal* **107**, 2112-2121
43. Vermaas, J. V., and Tajkhorshid, E. (2014) Conformational heterogeneity of α-synuclein in membrane. *Biochimica et Biophysica Acta (BBA)-Biomembranes* **1838**, 3107-3117
44. Bethoney, K. A., King, M. C., Hinshaw, J. E., Ostap, E. M., and Lemmon, M. A. (2009) A possible effector role for the pleckstrin homology (PH) domain of dynamin. *Proceedings of the National Academy of Sciences* **106**, 13359-13364
45. LEMMON, M. A., and FERGUSON, K. M. (2000) Signal-dependent membrane targeting by pleckstrin homology (PH) domains. *Biochemical Journal* **350**, 1-18
46. Lee, A., Frank, D. W., Marks, M. S., and Lemmon, M. A. (1999) Dominant-negative inhibition of receptor-mediated endocytosis by a dynamin-1 mutant with a defective pleckstrin homology domain. *Current biology* **9**, 261-265
47. Gervasio, F. L., Laio, A., and Parrinello, M. (2005) Flexible docking in solution using metadynamics. *Journal of the American Chemical Society* **127**, 2600-2607
48. Barducci, A., Bussi, G., and Parrinello, M. (2008) Well-tempered metadynamics: a smoothly converging and tunable free-energy method. *Physical review letters* **100**, 020603
49. Bonomi, M., Barducci, A., and Parrinello, M. (2009) Reconstructing the equilibrium Boltzmann distribution from well-tempered metadynamics. *Journal of computational chemistry* **30**, 1615-1621
50. Bonomi, M., and Parrinello, M. (2010) Enhanced sampling in the well-tempered ensemble. *Physical review letters* **104**, 190601
51. Dama, J. F., Parrinello, M., and Voth, G. A. (2014) Well-tempered metadynamics converges asymptotically. *Physical review letters* **112**, 240602
52. Chappie, J. S., Mears, J. A., Fang, S., Leonard, M., Schmid, S. L., Milligan, R. A., Hinshaw, J. E., and Dyda, F. (2011) A pseudoatomic model of the dynamin polymer identifies a hydrolysis-dependent powerstroke. *Cell* **147**, 209-222
53. Kozlov, M., Leikin, S., Chernomordik, L., Markin, V., and Chizmadzhev, Y. A. (1989) Stalk mechanism of vesicle fusion. *European Biophysics Journal* **17**, 121-129
54. Kozlovsky, Y., Chernomordik, L. V., and Kozlov, M. M. (2002) Lipid intermediates in membrane fusion: formation, structure, and decay of hemifusion diaphragm. *Biophysical journal* **83**, 2634-2651
55. Kozlovsky, Y., and Kozlov, M. M. (2002) Stalk model of membrane fusion: solution of energy crisis. *Biophysical journal* **82**, 882-895
56. Kozlovsky, Y., and Kozlov, M. M. (2003) Membrane fission: model for intermediate structures. *Biophysical journal* **85**, 85-96
57. Marrink, S. J., and Mark, A. E. (2003) The mechanism of vesicle fusion as revealed by molecular dynamics simulations. *Journal of the American Chemical Society* **125**, 11144-11145
58. Frolov, V. A., Escalada, A., Akimov, S. A., and Shnyrova, A. V. (2015) Geometry of membrane fission. *Chemistry and physics of lipids* **185**, 129-140
59. Kooijman, E. E., Chupin, V., de Kruijff, B., and Burger, K. N. (2003) Modulation of membrane curvature by phosphatidic acid and lysophosphatidic acid. *Traffic* **4**, 162-174
60. Fuhrmans, M., and Müller, M. (2015) Coarse-grained simulation of dynamin-mediated fission. *Soft matter* **11**, 1464-1480
61. Shchelokovskyy, P., Tristram-Nagle, S., and Dimova, R. (2011) Effect of the HIV-1 fusion peptide on the mechanical properties and leaflet coupling of lipid bilayers. *New journal of physics* **13**, 025004
62. Lai, C.-L., Srivastava, A., Pilling, C., Chase, A. R., Falke, J. J., and Voth, G. A. (2013) Molecular mechanism of membrane binding of the GRP1 PH domain. *Journal of molecular biology* **425**, 3073-3090
63. Yamamoto, E., Kalli, A. C., Yasuoka, K., and Sansom, M. S. (2016) Interactions of pleckstrin homology domains with membranes: adding back the bilayer via high-throughput molecular dynamics. *Structure* **24**, 1421-1431

64. Naughton, F. B., Kalli, A. C., and Sansom, M. S. (2018) Modes of interaction of pleckstrin homology domains with membranes: toward a computational biochemistry of membrane recognition. *Journal of molecular biology* **430**, 372-388
65. Srivastava, A., and Voth, G. A. (2014) Solvent-free, highly coarse-grained models for charged lipid systems. *Journal of chemical theory and computation* **10**, 4730-4744
66. Vonkova, I., Saliba, A.-E., Deghou, S., Anand, K., Ceschia, S., Doerks, T., Galih, A., Kugler, K. G., Maeda, K., and Rybin, V. (2015) Lipid cooperativity as a general membrane-recruitment principle for PH domains. *Cell reports* **12**, 1519-1530
67. Naughton, F. B., Kalli, A. C., and Sansom, M. S. (2016) Association of peripheral membrane proteins with membranes: free energy of binding of GRP1 PH domain with phosphatidylinositol phosphate-containing model bilayers. *The journal of physical chemistry letters* **7**, 1219-1224
68. Chan, K. C., Lu, L., Sun, F., and Fan, J. (2017) Molecular Details of the PH Domain of ACAP1BAR-PH Protein Binding to PIP-Containing Membrane. *The Journal of Physical Chemistry B* **121**, 3586-3596
69. Lemmon, M. A., Ferguson, K. M., O'Brien, R., Sigler, P. B., and Schlessinger, J. (1995) Specific and high-affinity binding of inositol phosphates to an isolated pleckstrin homology domain. *Proceedings of the National Academy of Sciences* **92**, 10472-10476
70. Ferguson, K. M., Lemmon, M. A., Schlessinger, J., and Sigler, P. B. (1995) Structure of the high affinity complex of inositol trisphosphate with a phospholipase C pleckstrin homology domain. *Cell* **83**, 1037-1046
71. Monticelli, L., Kandasamy, S. K., Periole, X., Larson, R. G., Tieleman, D. P., and Marrink, S.-J. (2008) The MARTINI coarse-grained force field: extension to proteins. *Journal of chemical theory and computation* **4**, 819-834
72. Marrink, S. J., De Vries, A. H., and Mark, A. E. (2004) Coarse grained model for semiquantitative lipid simulations. *The Journal of Physical Chemistry B* **108**, 750-760
73. Marrink, S. J., Risselada, H. J., Yefimov, S., Tieleman, D. P., and De Vries, A. H. (2007) The MARTINI force field: coarse grained model for biomolecular simulations. *The journal of physical chemistry B* **111**, 7812-7824
74. Jo, S., Kim, T., Iyer, V. G., and Im, W. (2008) CHARMM-GUI: a web-based graphical user interface for CHARMM. *Journal of computational chemistry* **29**, 1859-1865
75. Humphrey, W., Dalke, A., and Schulten, K. (1996) VMD: visual molecular dynamics. *Journal of molecular graphics* **14**, 33-38
76. Phillips, J. C., Braun, R., Wang, W., Gumbart, J., Tajkhorshid, E., Villa, E., Chipot, C., Skeel, R. D., Kale, L., and Schulten, K. (2005) Scalable molecular dynamics with NAMD. *Journal of computational chemistry* **26**, 1781-1802
77. Huang, J., Rauscher, S., Nawrocki, G., Ran, T., Feig, M., de Groot, B. L., Grubmüller, H., and MacKerell Jr, A. D. (2016) CHARMM36m: an improved force field for folded and intrinsically disordered proteins. *nature methods* **14**, 71
78. Klauda, J. B., Venable, R. M., Freites, J. A., O'Connor, J. W., Tobias, D. J., Mondragon-Ramirez, C., Vorobyov, I., MacKerell Jr, A. D., and Pastor, R. W. (2010) Update of the CHARMM all-atom additive force field for lipids: validation on six lipid types. *The journal of physical chemistry B* **114**, 7830-7843
79. Essmann, U., Perera, L., Berkowitz, M. L., Darden, T., Lee, H., and Pedersen, L. G. (1995) A smooth particle mesh Ewald method. *The Journal of chemical physics* **103**, 8577-8593
80. Lomize, M. A., Lomize, A. L., Pogozheva, I. D., and Mosberg, H. I. (2006) OPM: orientations of proteins in membranes database. *Bioinformatics* **22**, 623-625
81. Leong, S., Lim, T., and Choong, Y. (2016) Bioinformatics for Membrane Lipid Simulations: Models, Computational Methods, and Web Server Tools. in *Bioinformatics-Updated Features and Applications*, InTech. pp
82. Pettersen, E. F., Goddard, T. D., Huang, C. C., Couch, G. S., Greenblatt, D. M., Meng, E. C., and Ferrin, T. E. (2004) UCSF Chimera—a visualization system for exploratory research and analysis. *Journal of computational chemistry* **25**, 1605-1612

83. Ferguson, K. M., Lemmon, M. A., Schlessinger, J., and Sigler, P. B. (1994) Crystal structure at 2.2 Å resolution of the pleckstrin homology domain from human dynamin. *Cell* **79**, 199-209
84. Zoete, V., Cuendet, M. A., Grosdidier, A., and Michielin, O. (2011) SwissParam: a fast force field generation tool for small organic molecules. *Journal of computational chemistry* **32**, 2359-2368
85. Pymol, T. (2010) The PyMOL molecular graphics system. Version
86. Bussi, G., Donadio, D., and Parrinello, M. (2007) Canonical sampling through velocity rescaling. *The Journal of chemical physics* **126**, 014101
87. Parrinello, M., and Rahman, A. (1981) Polymorphic transitions in single crystals: A new molecular dynamics method. *Journal of Applied physics* **52**, 7182-7190
88. Hess, B. (2008) P-LINCS: A parallel linear constraint solver for molecular simulation. *Journal of Chemical Theory and Computation* **4**, 116-122
89. Abraham, M. J., Murtola, T., Schulz, R., Páll, S., Smith, J. C., Hess, B., and Lindahl, E. (2015) GROMACS: High performance molecular simulations through multi-level parallelism from laptops to supercomputers. *SoftwareX* **1**, 19-25
90. Tribello, G. A., Bonomi, M., Branduardi, D., Camilloni, C., and Bussi, G. (2014) PLUMED 2: New feathers for an old bird. *Computer Physics Communications* **185**, 604-613

FOOTNOTES

Financial support from the Indian Institute of Science-Bangalore and the high-performance computing facility ‘‘Arjun’’ setup from grants by a partnership between the Department of Biotechnology of India and the Indian Institute of Science are greatly acknowledged. A.S. thanks the startup grant provided by the Ministry of Human Resource Development of India and the early career grant from the Department of Science and Technology of India.

The abbreviations used are: PHD, pleckstrin homology domain of dynamin protein; CG coarse grain; HMMM, Highly Mobile Membrane-Mimetic Model; VL, variable loop; MD, molecular dynamics

Systems	Bending Modulus (k_BT)
Pure Membrane	21.22
PHD(WT)-Membrane	13.35
PHD(I533A)-Membrane	16.83
PHD(F579A)-Membrane	15.46
PHD(K539A + K583A)-Membrane	14.61

Table 1: Values of bending modulus for different membrane systems obtained by fitting the undulation spectra to Helfrich theory (no curvature-undulation coupling). The membrane systems (25 nm by 25 nm area) is made up of 2048 CG lipids and 14 randomly placed PHDs on one leaflet.

Name	PHD orientation on the bilayer	# Simulation time (ns)
Conf1	Inverted (Fig. 3a)	100+
Conf2	Inverted (Fig. 3d)	100+
Conf3	VL1 near PIP_2 (Fig. S4a)	100
Conf4	VL4 near PIP_2 (Fig. S4d)	100
Conf5	VL3 near PIP_2	100
Conf6	VL1 near PIP_2	100
Conf7	VL3 near PIP_2	100
Conf8	VL4 near PIP_2	100

Table 2: Eight different HMMM systems were created with different initial poses for PHD on the mimetic membrane. In Conf1 and Conf2 systems, the membrane binding loop regions were facing away from the membrane surface while Conf3 and Conf4, the PIP_2 and specific loops were biased towards the binding pockets. Conf5-Conf8 were other configurations with scrambled initial orientations.

DOPC-DOPS-PIP2 (80:19:1)	DOPC-DOPS (60:40)	DOPC-DOPS (80:20)
WT	WT	WT
I533A	I533A	I533A
F579A	F579A	F579A
Y600L	K539A	K539A
K583A	K583A	K583A
K539A and K583A	-	-

Table 3: Details of variants of PHD used for all-atom membrane simulations with different lipid compositions

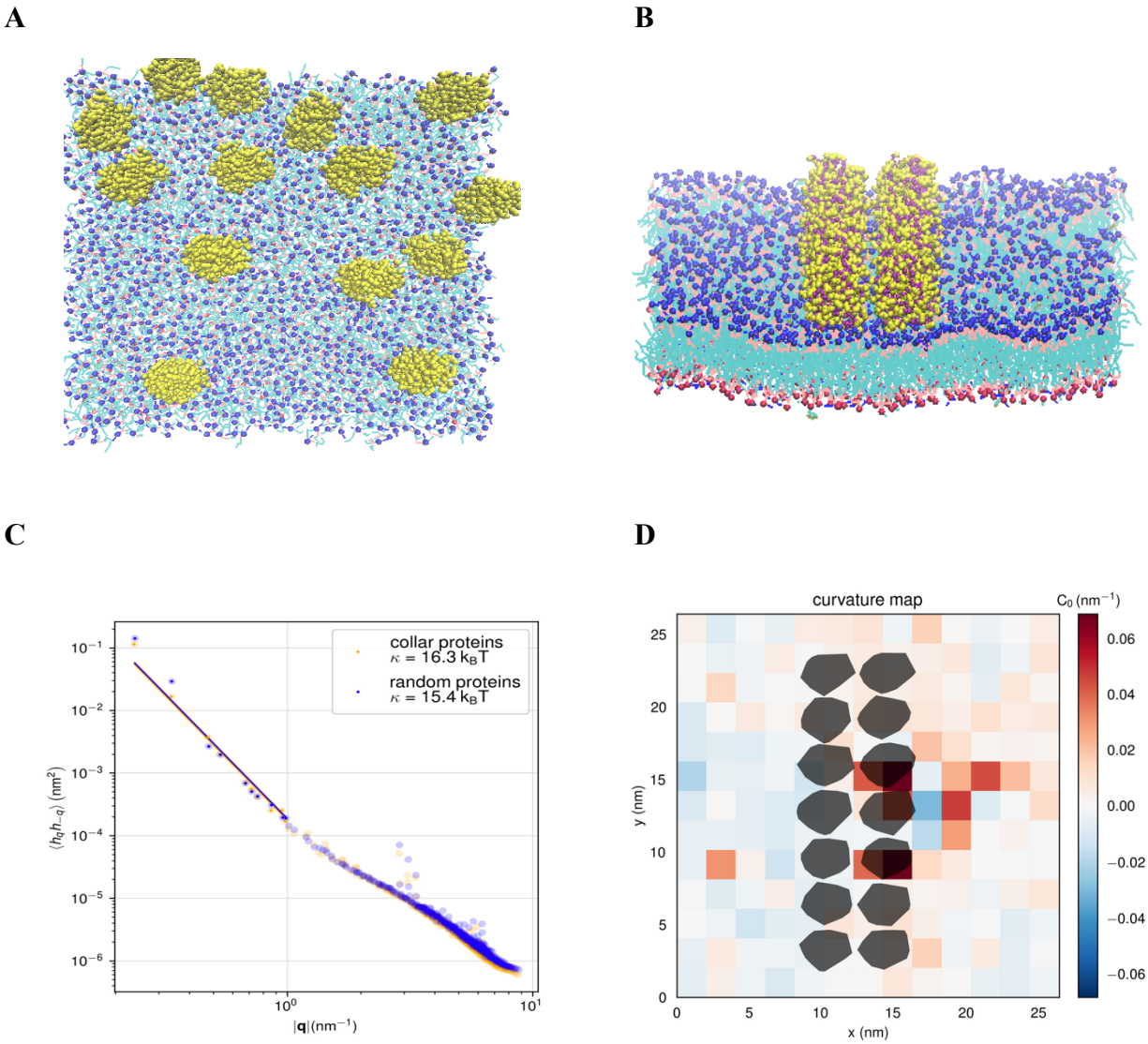

Figure 1. (A) Snapshot (top view) from a Martini CG system with 2048 lipids and 14 CG PHDs (shown in yellow) distributed randomly on the bilayer surface. (B) The PHDs are arranged in a collar on the membrane surface (front view) The PO4 on upper leaflet is shown in blue and on lower leaflet in red (C) Height-height undulation spectra for the two systems shown above according to equation 1. The undulation spectra follow the standard Helfrich type $\mathbf{q}^4$ scaling and the effect of curvature on bending modulus is not significant. Full fluctuation spectra for coarse-grained systems comprising of 2048 lipids with pure membrane (no PHD) and membrane with 14 PHD are shown in Fig S1. (D) Averaged curvature fields for bilayers with 14 PHDs does not show any strong curvature propensity despite the PHDs arranged in collar format.

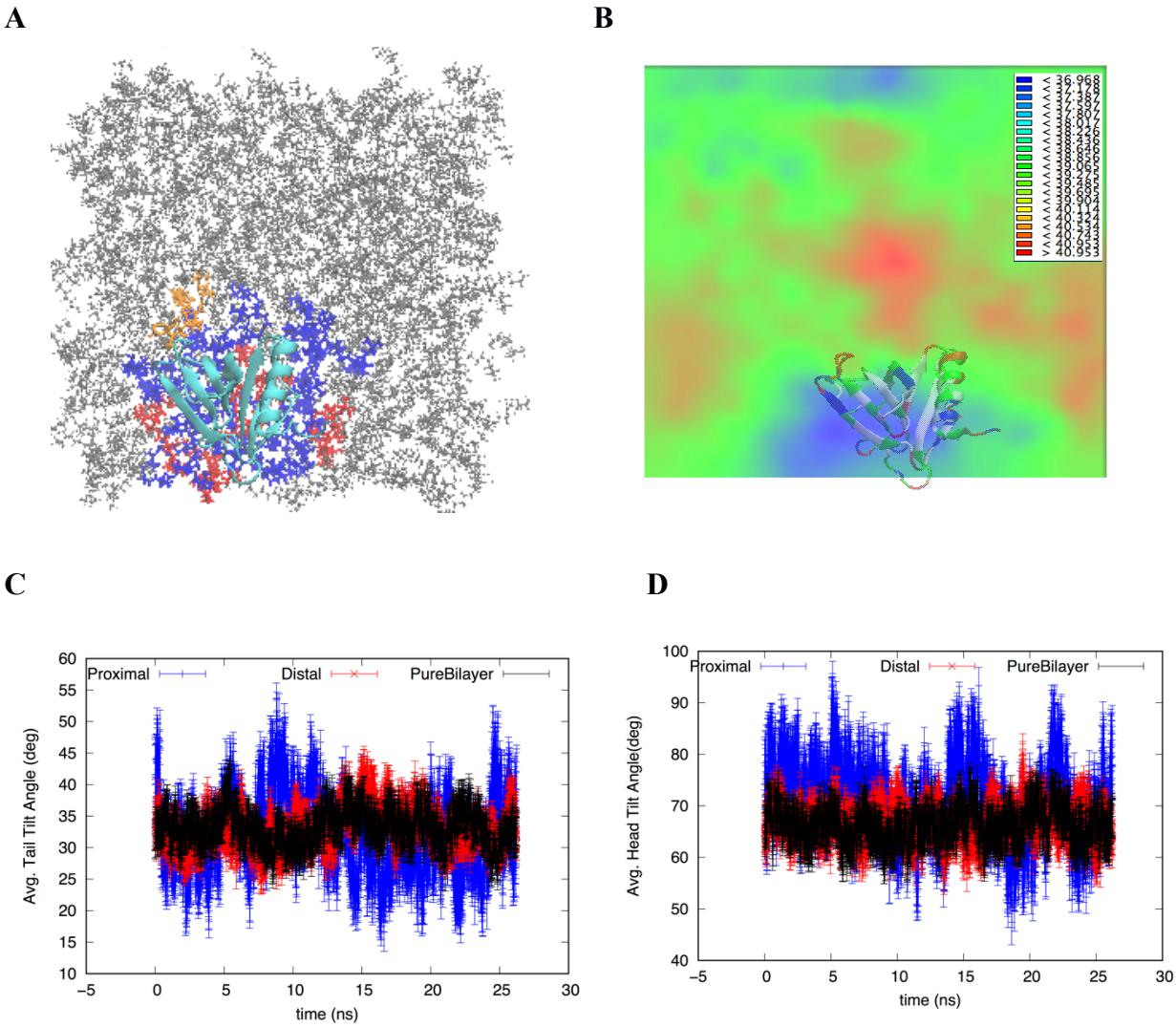

Figure 2. (A) Snapshot from an all-atom DOPC-DOPS-PIP_2 bilayer system with single PHD (shown in cyan) on the upper leaflet. The lipids proximal to the protein are marked in blue (DOPC), red (DOPS) and orange PIP_2. The distal lipids are marked in grey. The lipids were tracked for 500 ns for the analysis (B) The average thickness profile of the bilayer with the PHD showing thinner regions in blue and thicker regions in red. (C) Average tail angle for lipids proximal to the protein (blue), distal to the protein (red) and in pure bilayer with no proteins (black) (D) Average head angle for lipids

A

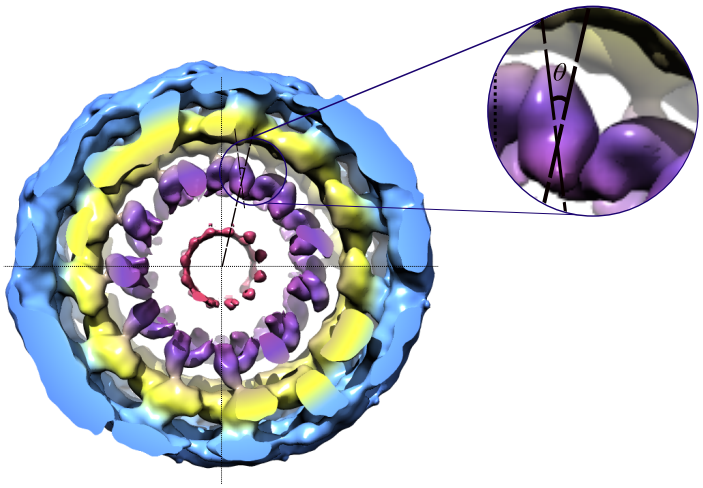

B

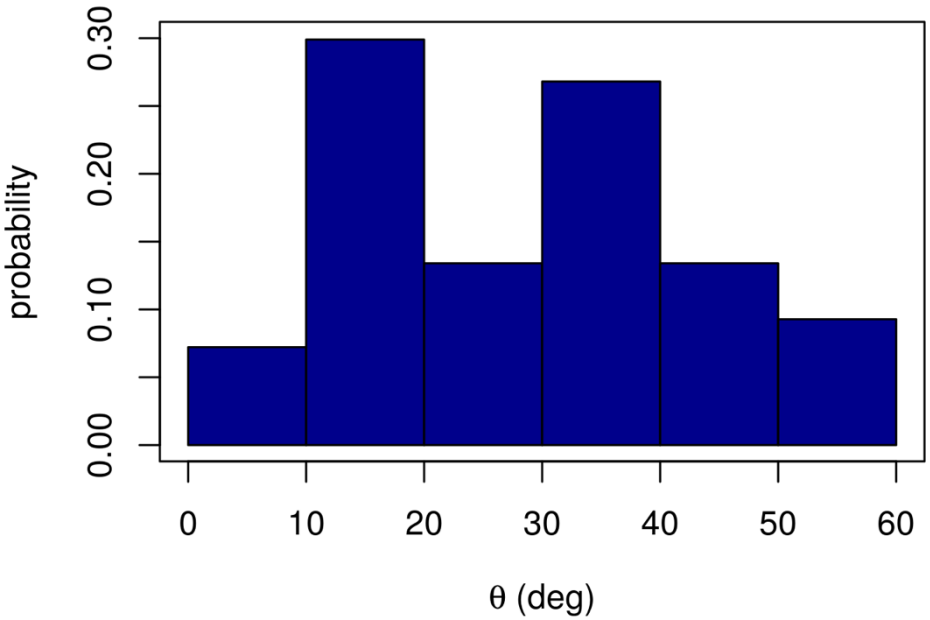

Figure 3. (A) End view of the 3D density map of dynamin polymer assembled on the membrane. The radial densities colored in purple shows the PHDs on the collar. The inset show the angle that the end to end vector of given PHD makes with the radial line passing through the centres of the tube and the given PHD. The density map is re-drawn from the available cryo-EM density data by Jennifer Hinshaw and co-workers (B) The probability distribution of angle described above in the cryo-EM map. The angle θ has a wide range for the constricted collar.

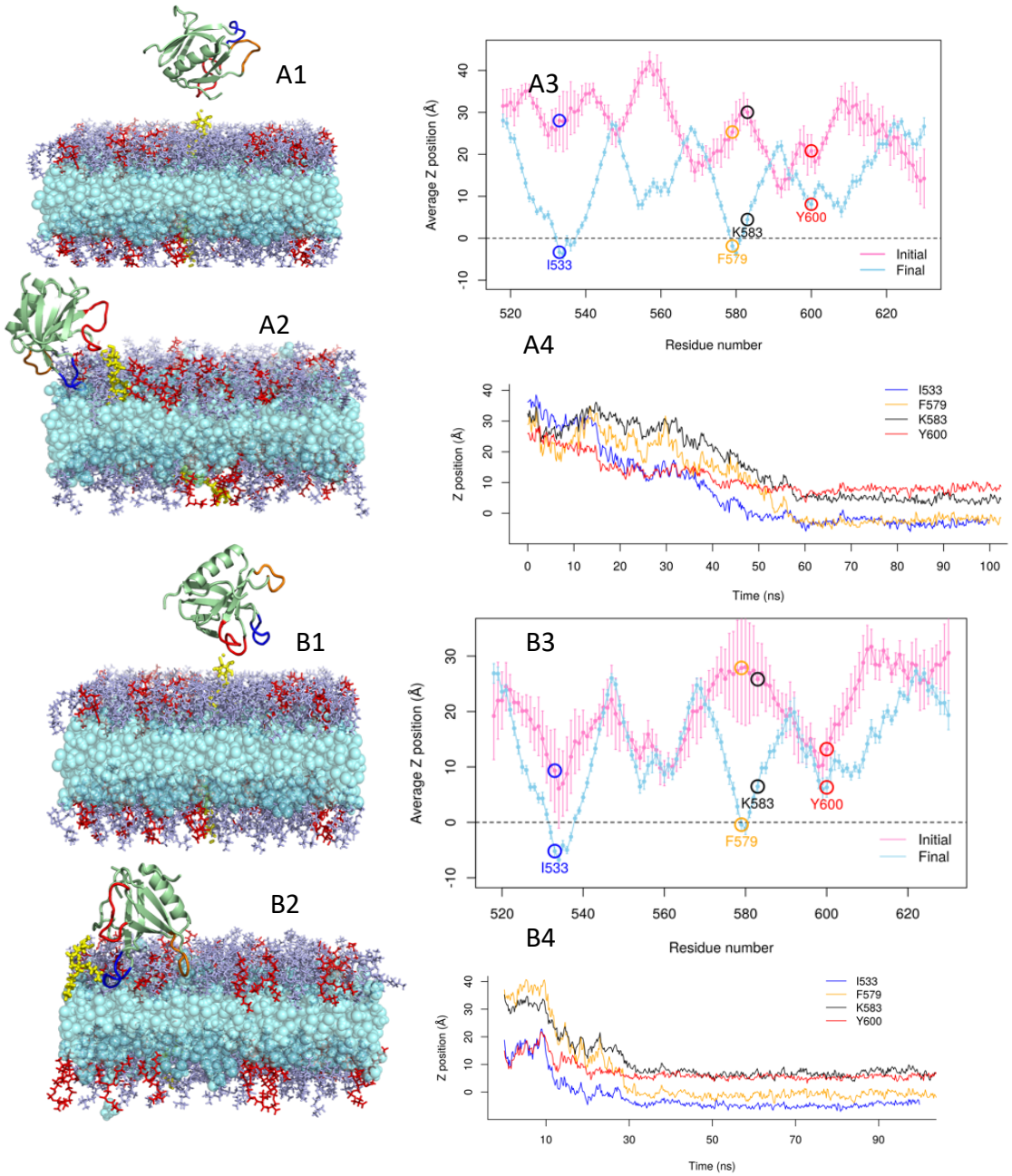

Figure 4. The two contrasting orientations (out of eight) shown for HMMM simulations. The PC, PS and PIP mimetic lipids are shown in glass blue, red and yellow, respectively. DCLE is shown in light green in the core of the bilayer. The VL1 of PHD is shown in blue, VL3 in red and VL4 is shown in orange color. The top two left panel show the initial (A1) and final (A2) PHD orientations with an "inverted" starting configuration. The panel (B1) shows initial orientations with VL1 and VL3 closer to the membrane surface and the converged orientations is shown in panel B2. The initial and final z-positions (distance from phosphate plane) for all residues for both systems are shown in panel A3 and panel B3, respectively for the two starting orientations. The time evolutions of membrane associations for key residues (I553 in VL1, Y600 in VL3 and I579 and I583 in VL4, are shown in panel A4 and B4 for the two systems.

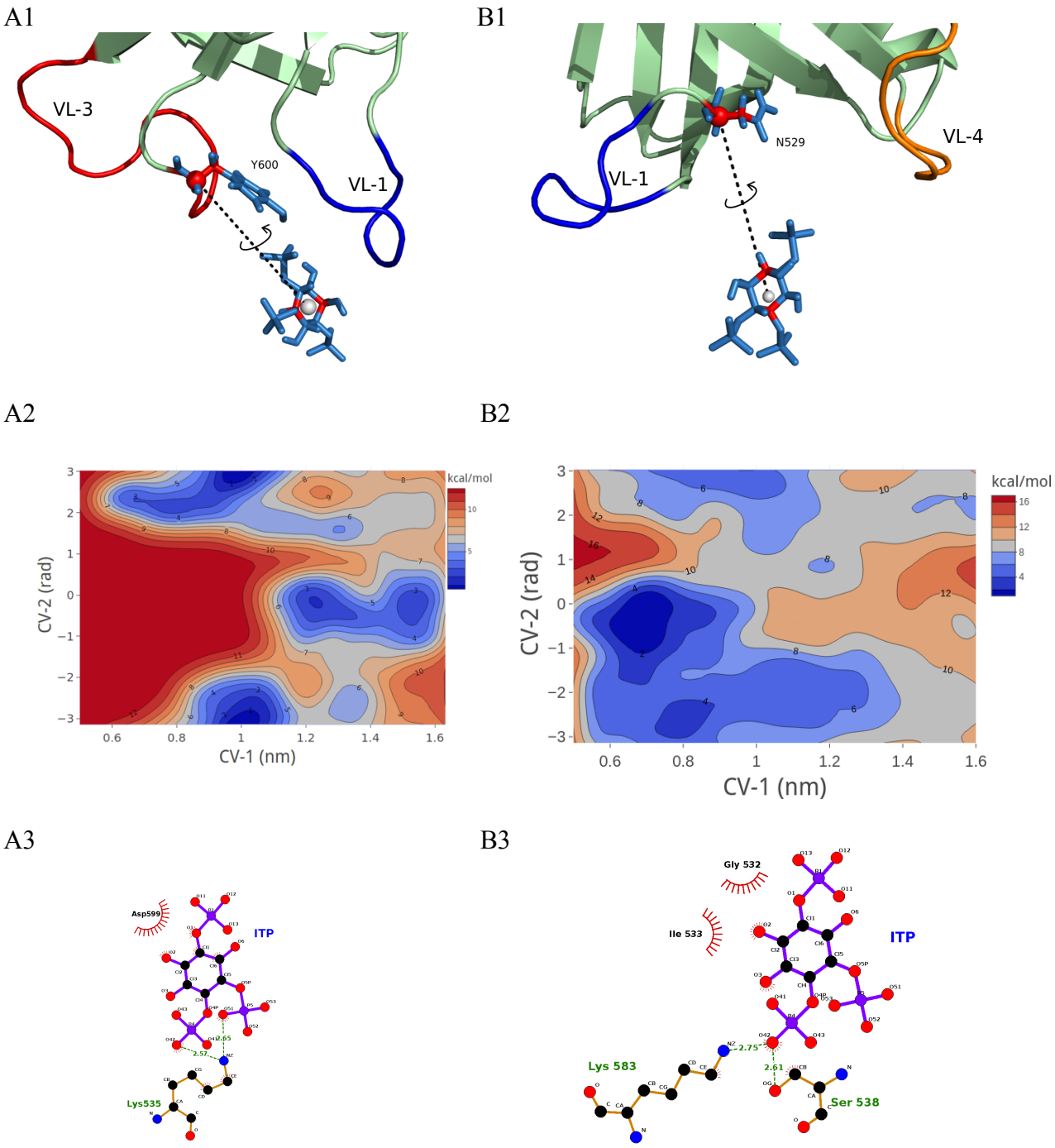

Figure 5. Plain metadynamics setup with docking region for IP_3 ligand biased towards VL1 and VL3 loops (A1) and towards VL1 and VL4 (B1). The free energy landscape for the two systems are shown in panels A2 and B2, respectively. The plots showing the converge of these calculations are shown in SI. Panels A3 and B3, shows the ligplot of the ligand-protein association at the lowest free energy basin. Due to the degenerate nature of the free energy surface, several other geometries are viable as discussed (data shown in SI).

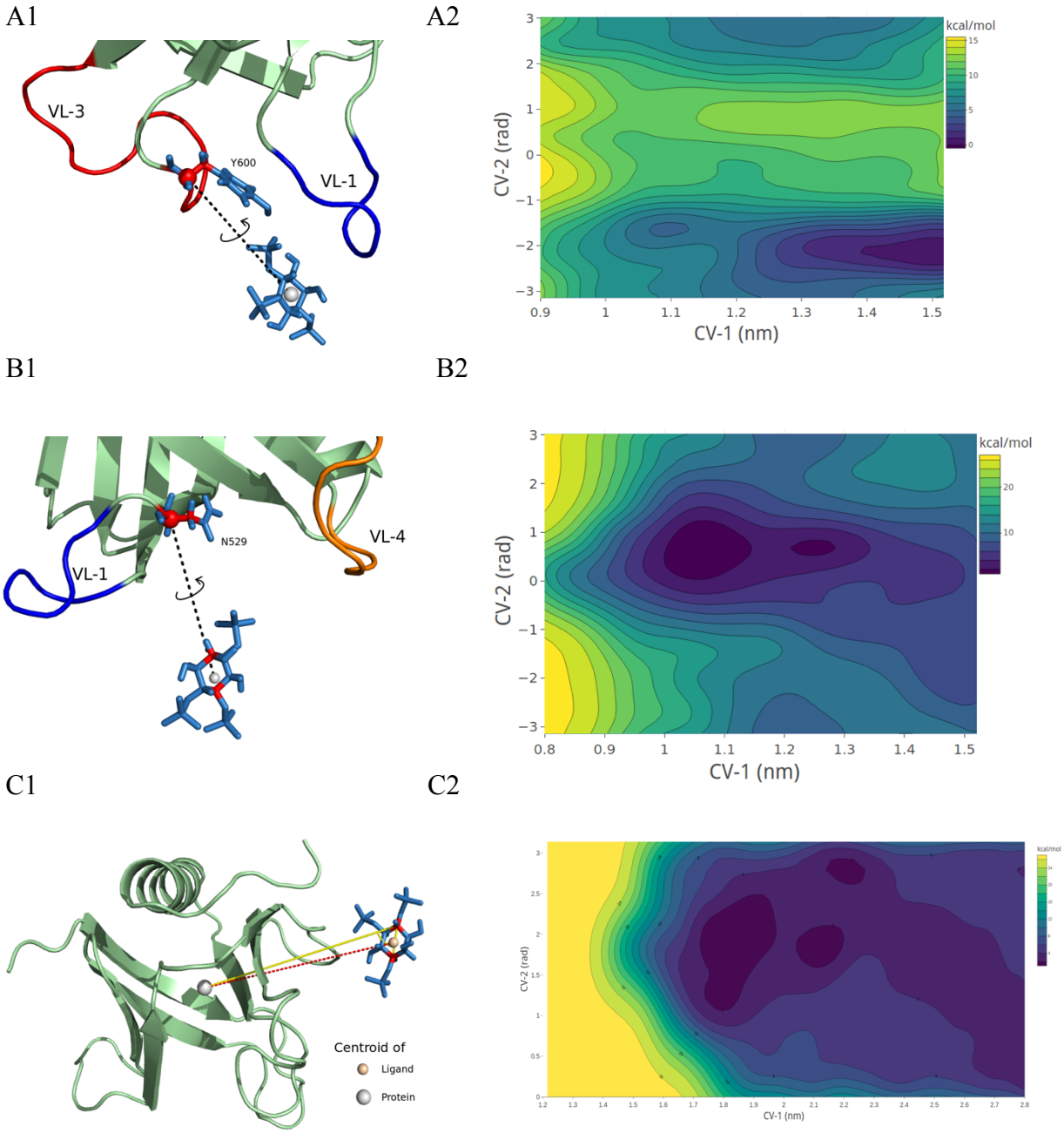

Figure 6. Well-tempered metadynamics setup with docking region for IP_3 ligand biased towards VL1 and VL3 loops (A1), towards VL1 and VL4 loops (B1) and with no bias towards any loop region (C1). The free energy landscape for the three systems are shown in panels A2, B2 and C2, respectively. The lowest energy configurations are picked from the lowest basins and regions free energy difference of <2kT from the minimum basin. Several orientations of IP3 bound states are found as shown in the next figure.

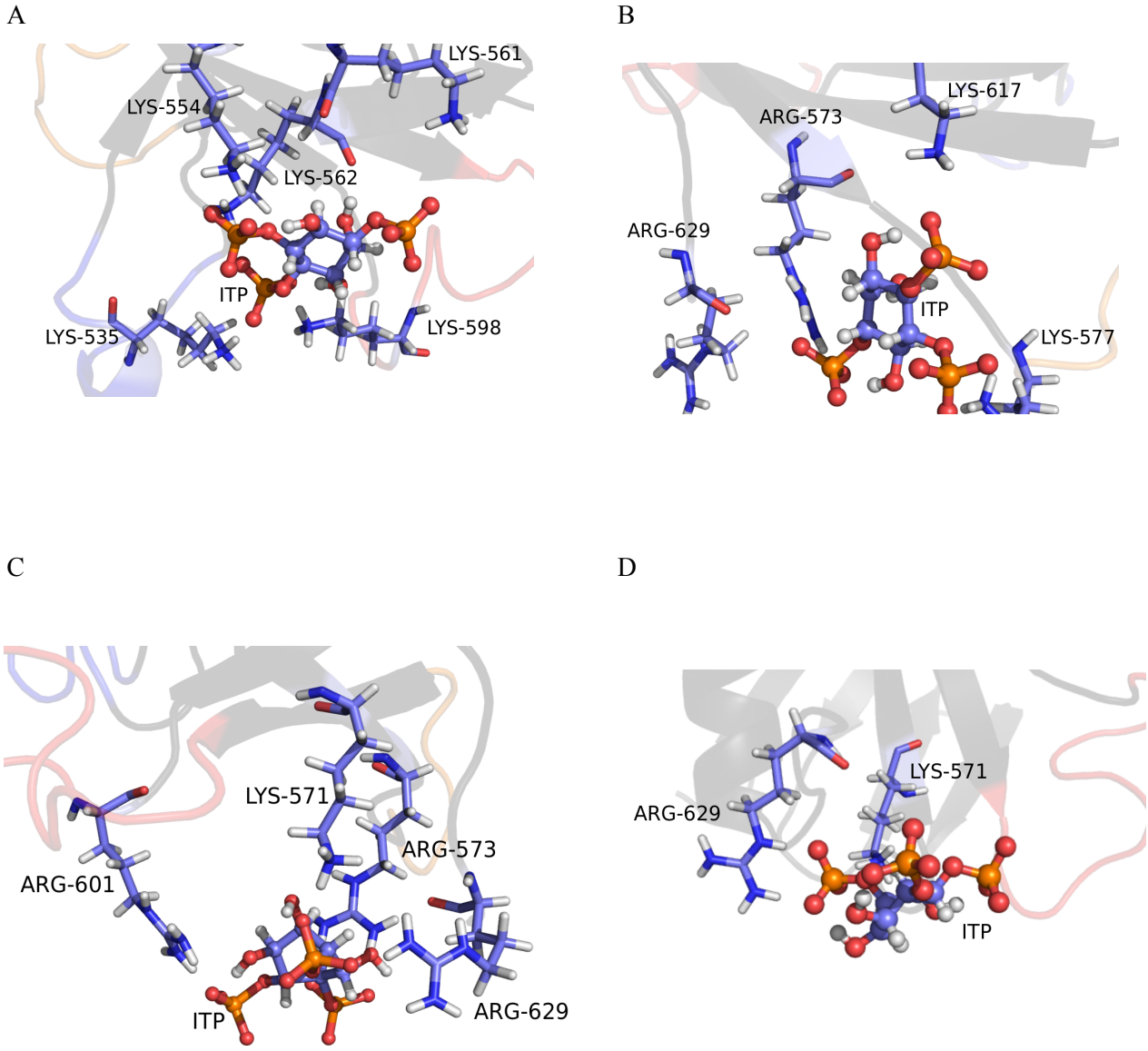

Figure 7: Binding geometries for the PIP_2 headgroup with the PHD. IP3 is represented as ball and stick and associating residues are shown in sticks. Nitrogen, Oxygen, Carbon, Hydrogen and Phosphorus are represented as dark blue, red, light blue, white and orange, respectively. The docking profiles are shown for three different systems where A, B and C correspond to A1, B1, and C1 systems, respectively from Fig. 6.

A

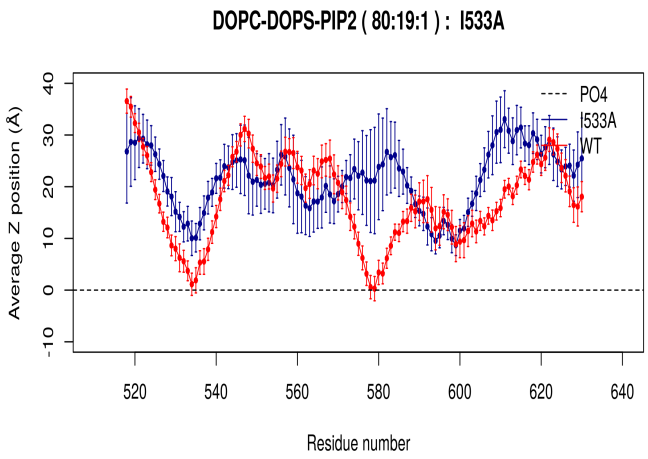

B

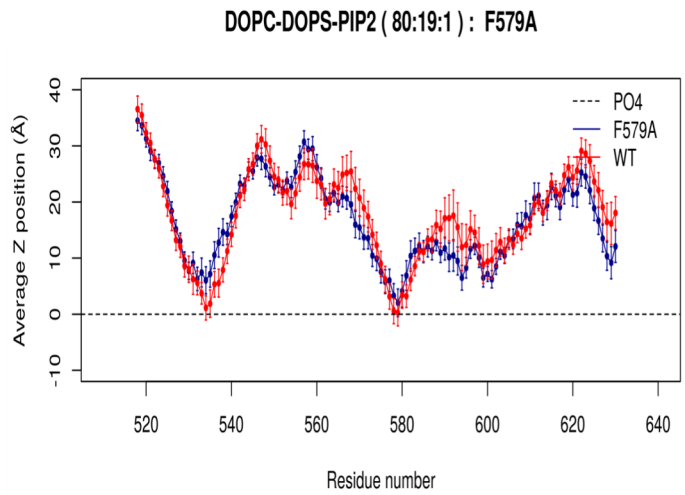

C

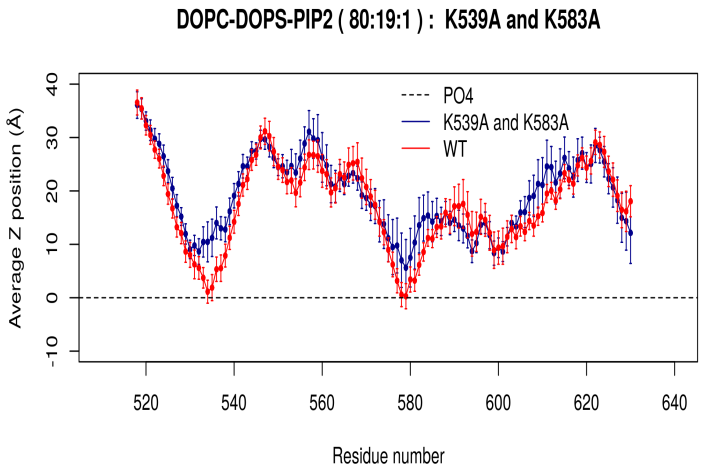

Figure 8. Effect of mutations captured using full atomistic simulations - Position of residues of PHD on the basis of Z-distance calculated for : A) I533A mutation in VL1 b) K579A mutation in VL4 C) Double mutation K539A (VL1) and K583A (VL4). Similar calculations were carried out on other systems (listed in Table 3) and some of the results are reported in SI.

Supporting Information

Flexible pivoting of the PH domain in dynamin catalyzes fission by affecting membrane properties: Insights into the molecular degrees of freedom

Kirtika Jha[1†], Krishnakanth Baratam[1†], Vikas Dubey[1], Thomas J. Pucadyil[2] and Anand Srivastava[1]*

From the [1]Molecular Biophysics Unit, Indian Institute of Science, Bangalore, Karnataka, India 560012; [2]Indian Institute of Science Education and Research, Dr. Homi Bhabha Road, Pashan, Pune, Maharashtra, India 411008

Running title: *Dynamics of the membrane-bound dynamin PHD*

† Contributed equally

* To whom correspondence should be addressed: Anand Srivastava: Molecular Biophysics Unit, Biological Sciences Division, Indian Institute of Science, Bangalore, Karnataka, India 560012; anand@iisc,ac.in; Tel. +91-80-2293-3552; Fax. +91-80-2360-0535.

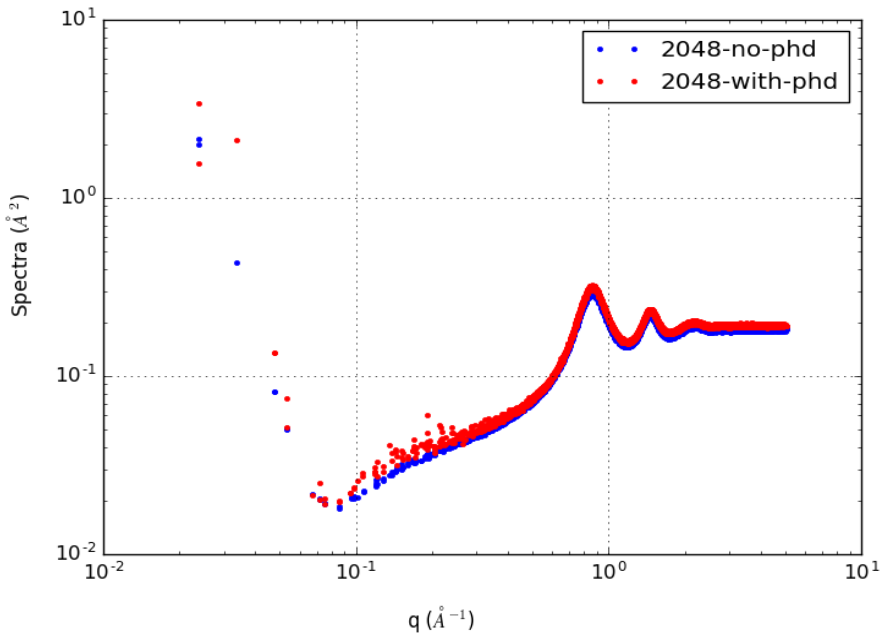

Figure S1: Undulation spectra of CG bilayer (2048 lipids Martini forcefield). Pure bilayer spectra is shown in blue while the spectra with 14 PHDs on the top leaflet (randomly arranged) is shown in red.

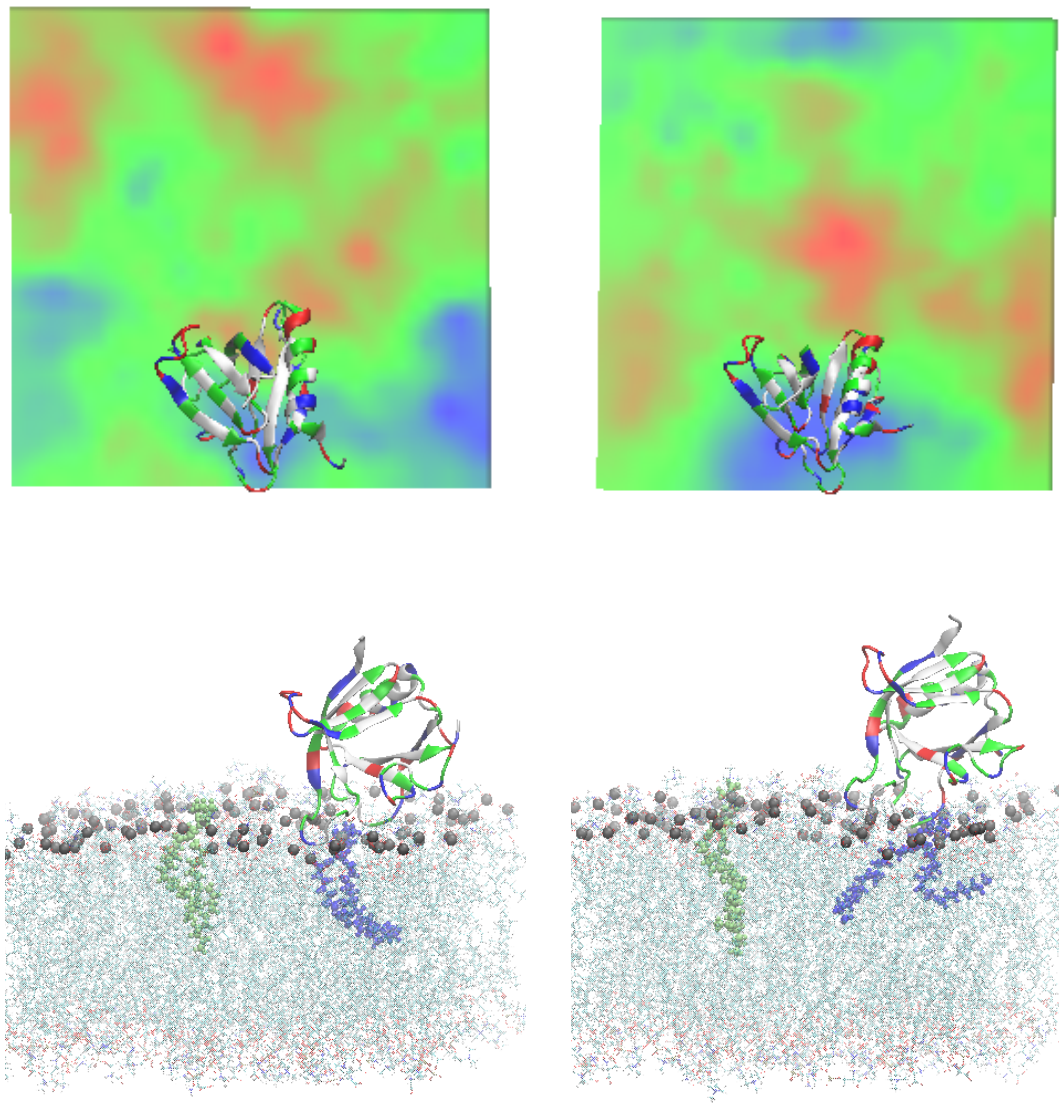

Figure S2: Top panel shows the membrane thickness profile for two other systems with dyn-PHD on all-atom bilayer. The difference between the thinnest and thickest regions is around 0.4 nm. The bottom panel shows snapshot of a PHD-bilayer run and the blue lipid denotes a dyn-PHD proximal lipid while the green color shows the distal lipid. The proximal lipid has a visible tilt (left bottom) and very noticeable splay. The average statistical data for the splay and tilt are shown in Fig. 2.

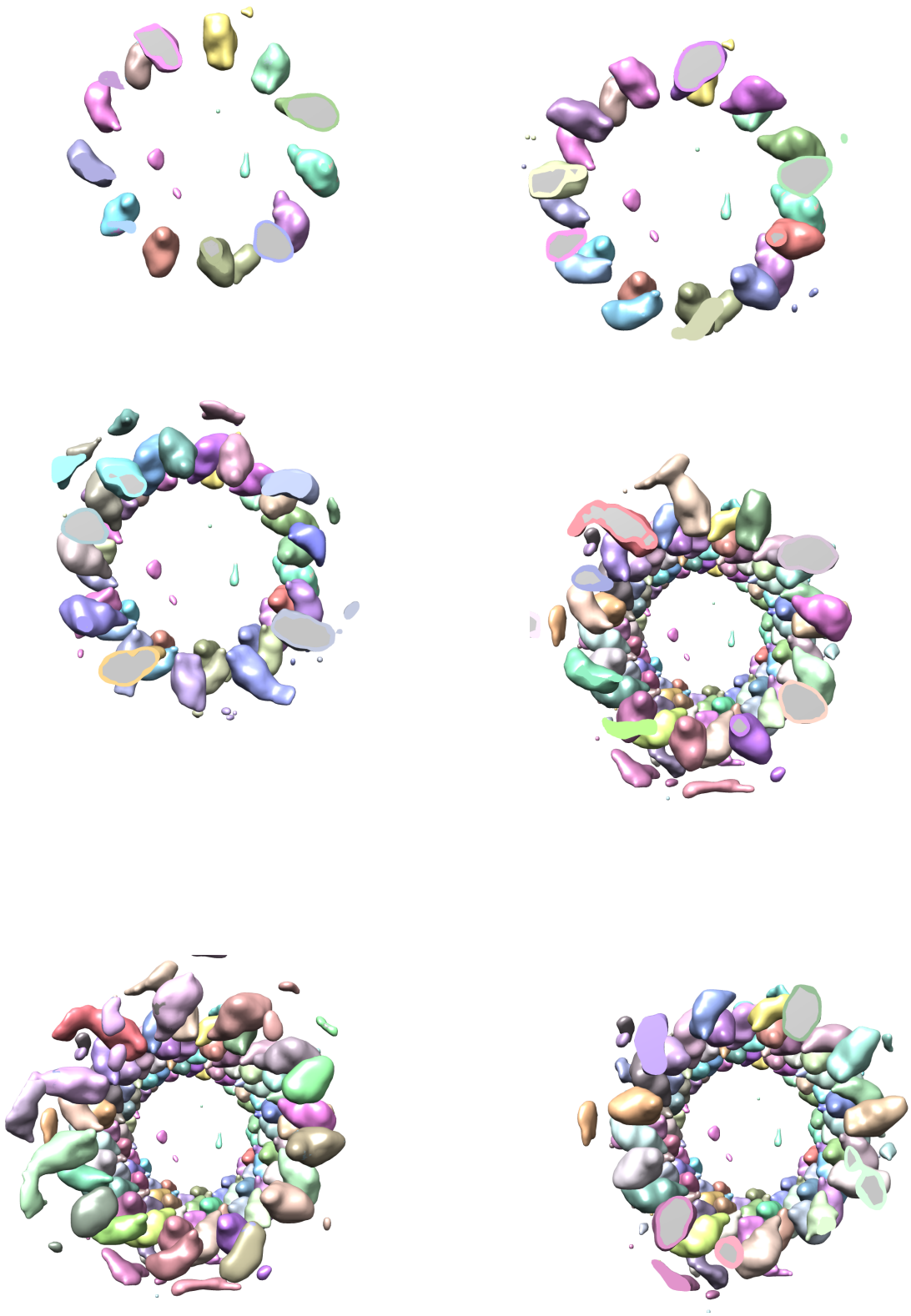

Figure S3: End view of the 3D density map of dynamin polymer assembled on the membrane. The top-left panel shows the front most slice of the scaffold with dyn-PHDs in different orientations. The right-bottom panel shows the full scaffold. The density map is re-drawn from the available cryo-EM density data by Jennifer Hinshaw and co-workers

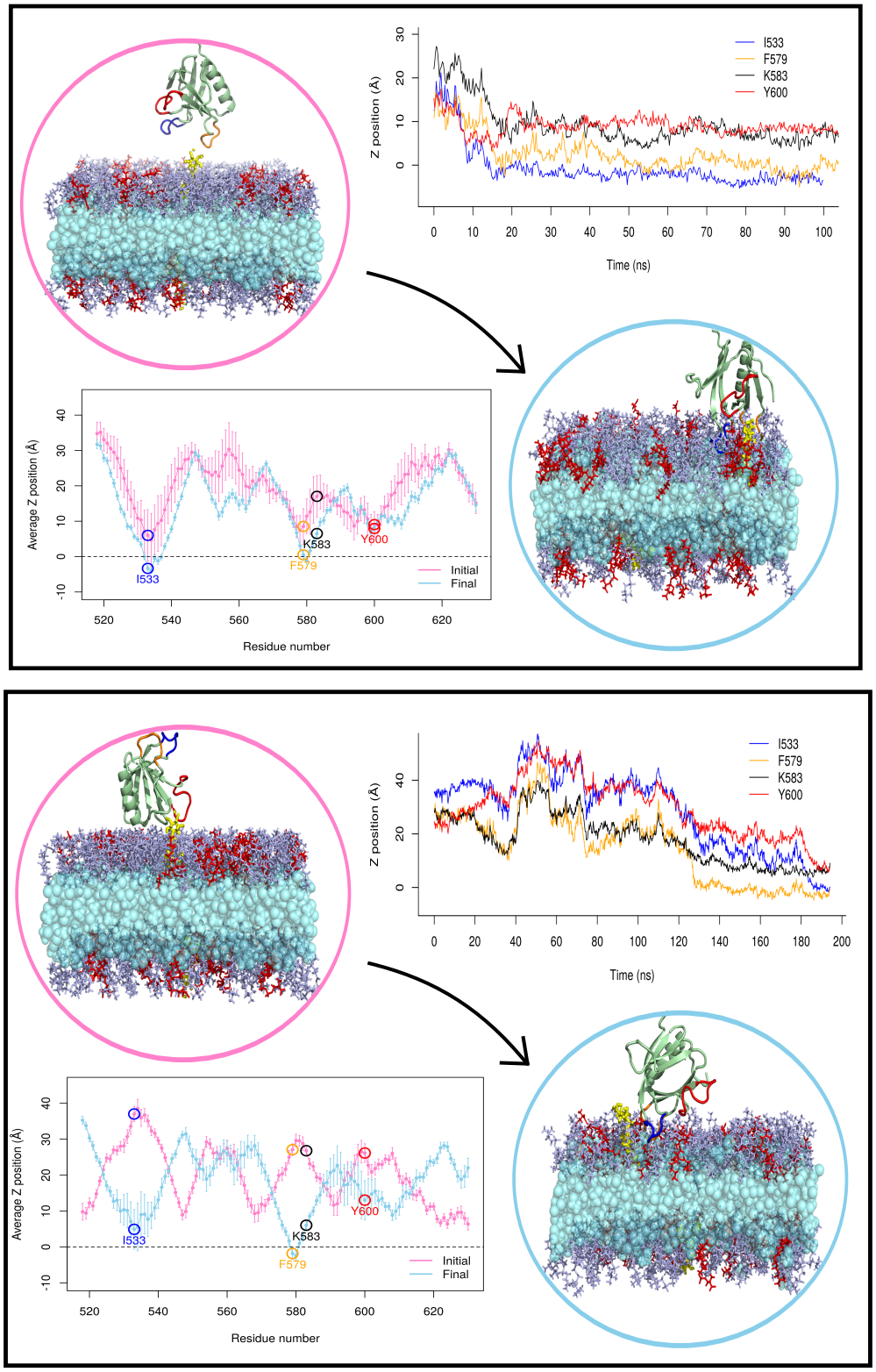

Figure S4: The top panel show the HMMM simulation with dyn-PHD orientations with an starting configuration having VL1 and VL4 loops facing the membrane. The bottom panel has VL1 and VL4 far away from the membrane and in inverted configuration. Both cases converge to membrane-protein configuration profile that favours VL1 and VL4 loops in membrane association, with different overall orientation of the domain.

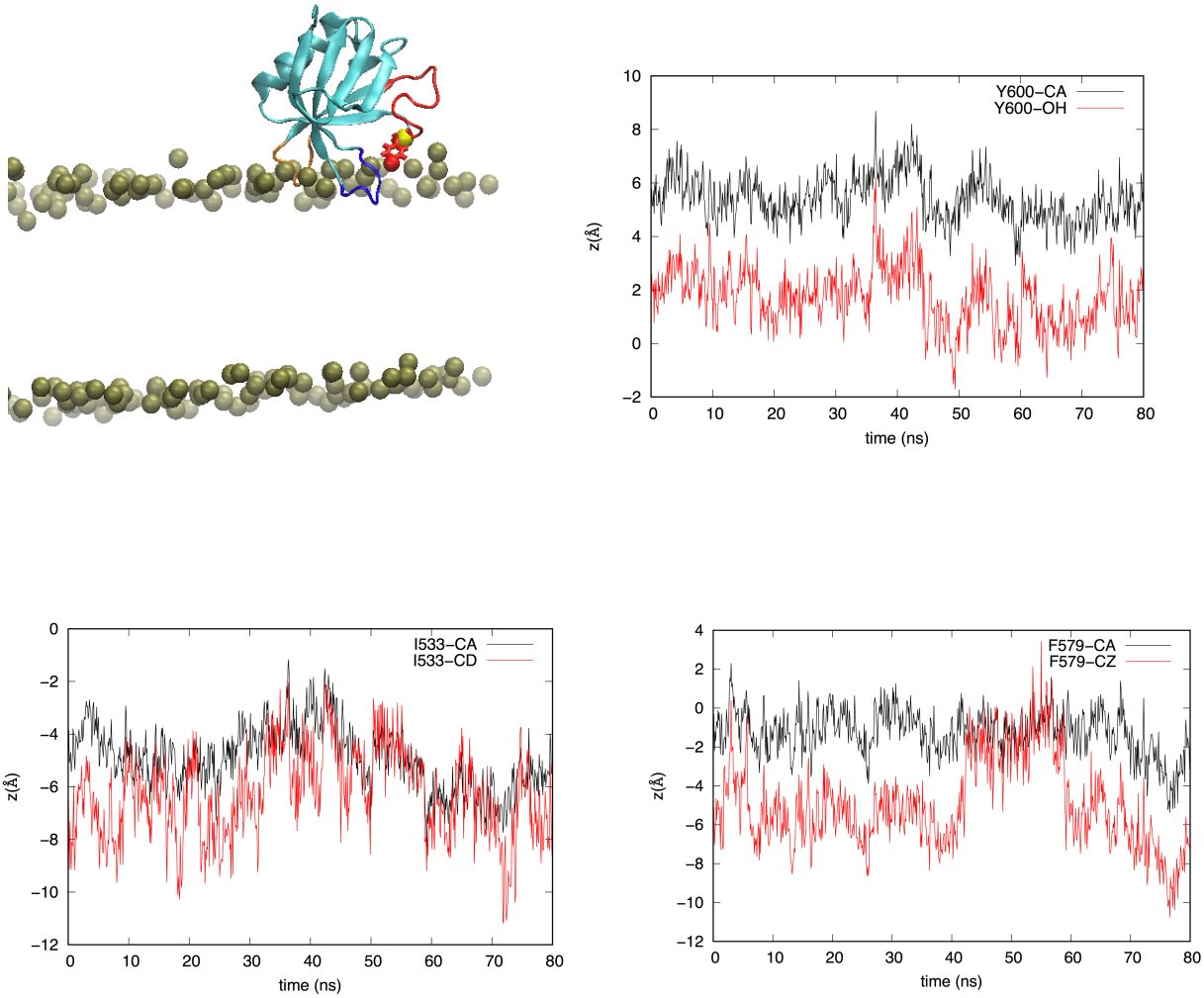

Figure S5: The top left panel shows snapshot of a dyn-PHD on HMMM bilayer with membrane phosphorus shown in the figure. The loops are colored as blue (VL1), red (VL3) and orange (VL4). Top right shows how the z-distance of Y600 (VL3) evolves with time for the C-alpha atom and the terminal OH site on the side chain. This shows that the side chain is buried deeper though C-alpha analysis of Y600 shows the residue to be a slightly away from the membrane surface. Similar analysis was carried out for other mutants and the results for I533 (VL1) and I579 (VL4) are shown in bottom panel.

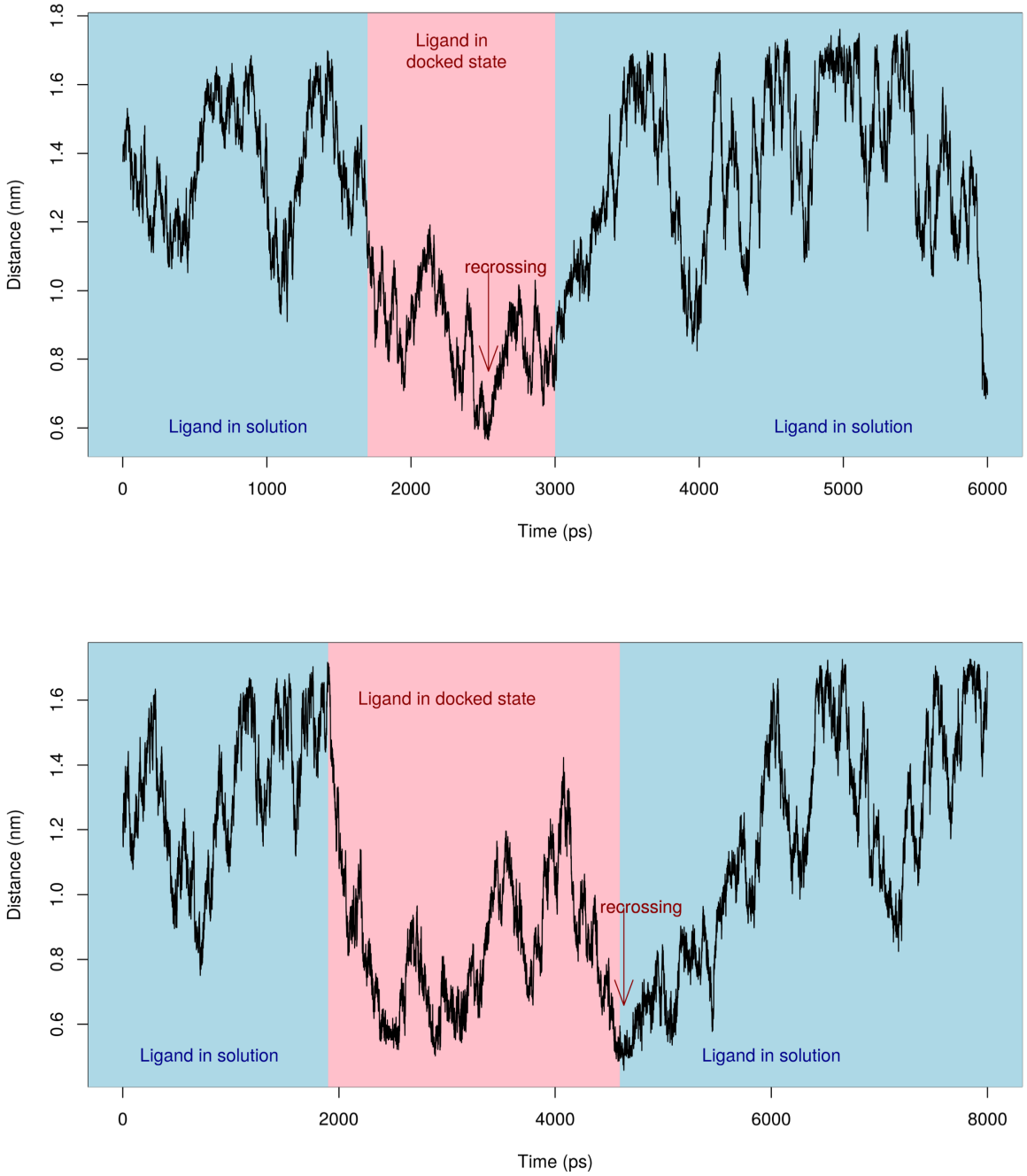

Figure S6: The distance between IP3 ligand and dyn-PHD as a function of time. The re-crossing time point in this plain metadynamics runs is shown with a red arrow and the free energy surface is plotted at that instant of time. (Top) The distance is between the center of inositol and C-alpha atom of TYR600 with with a docking bias towards the pockets formed between loops VL1 and VL3 loops. (Bottom) The distance is between the center of inositol and C-alpha atom of ASN529 with a docking bias towards the pockets formed between loops VL1 and VL4 loops

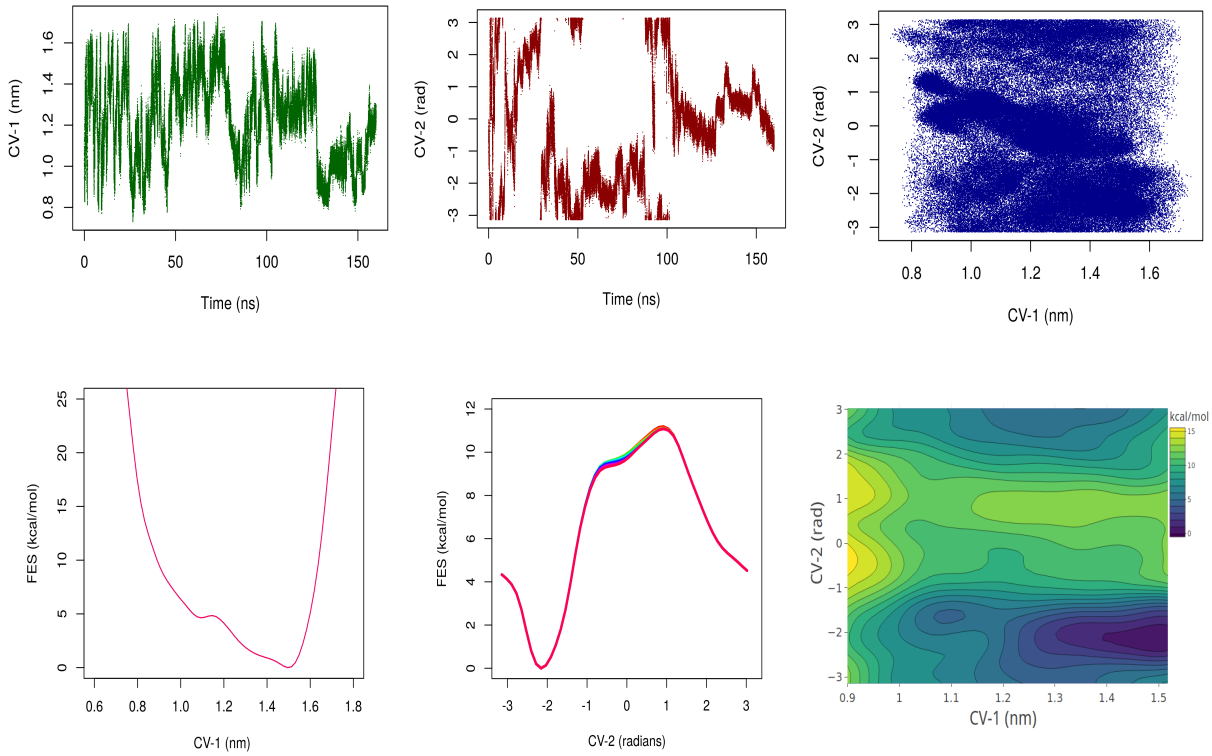
CV-1 (nm)
Time (ns)
CV-2 (rad)
Time (ns)
CV-2 (rad)
CV-1 (nm)
FES (kcal/mol)
CV-1 (nm)
FES (kcal/mol)
CV-2 (radians)
CV-2 (rad)
CV-1 (nm)
kcal/mol

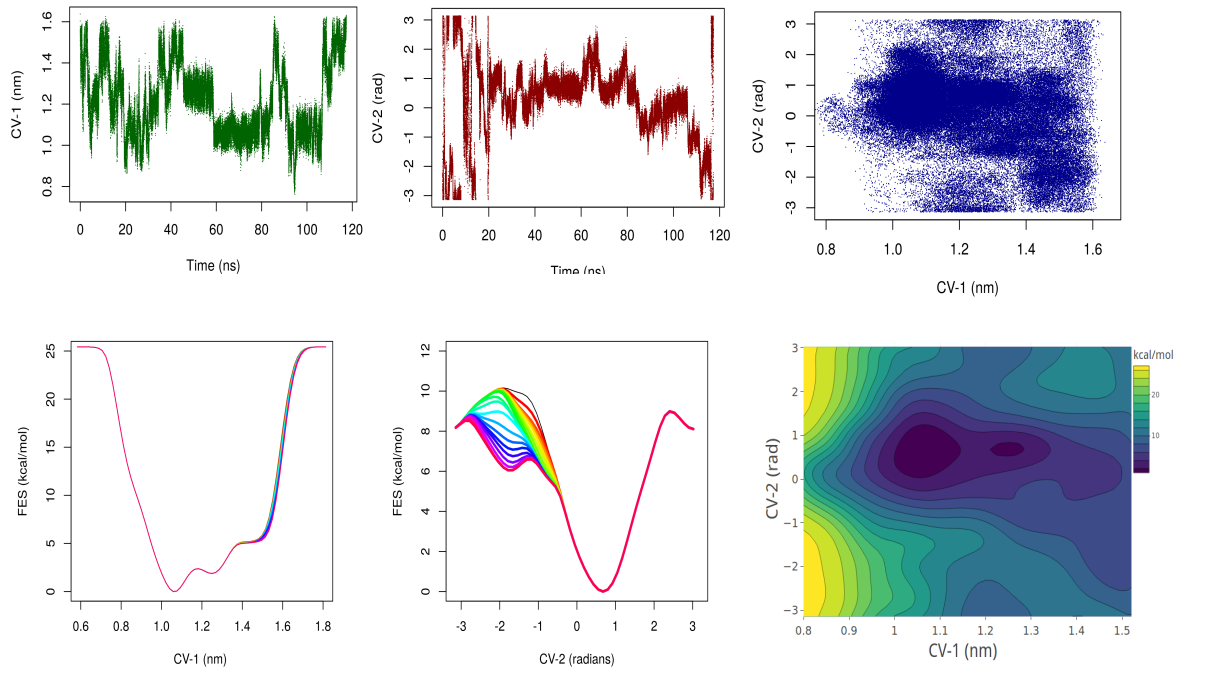
CV-1 (nm)
Time (ns)
CV-2 (rad)
Time (ns)
CV-2 (rad)
CV-1 (nm)
FES (kcal/mol)
CV-1 (nm)
FES (kcal/mol)
CV-2 (radians)
CV-2 (rad)
CV-1 (nm)
kcal/mol

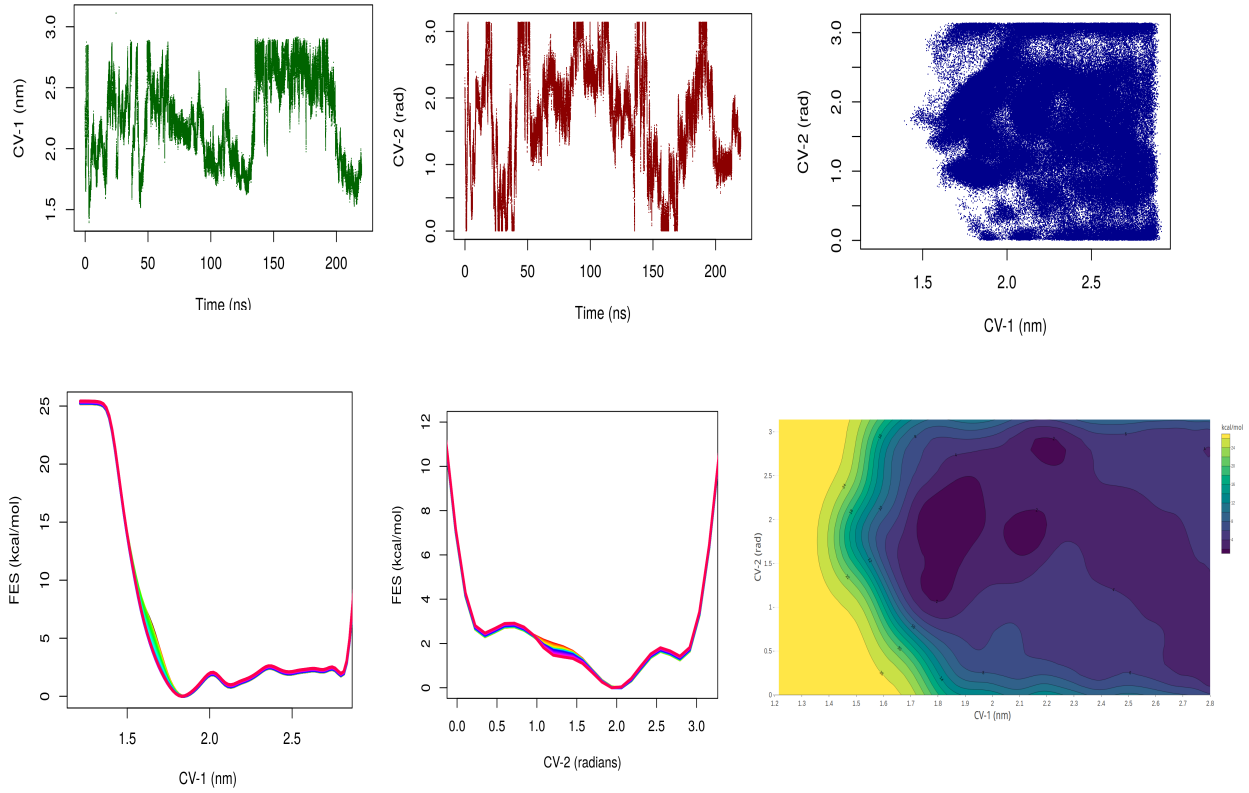

Figure S7: Convergence analysis for the well-tempered metadynamics runs. Top panel shows convergence results for simulations where with VL1-VL3 was chosen as the preferred docking area, middle panel is for system with VL1-VL4 as the preferred pocket and the bottom most panel is for system with no bias for any pocket. Top row for each panel shows the time evolution (sampling) of individual CV as well as both together. The bottom row for each panel shows the free energy surface (FES) data for individual CVs as well as when put together.

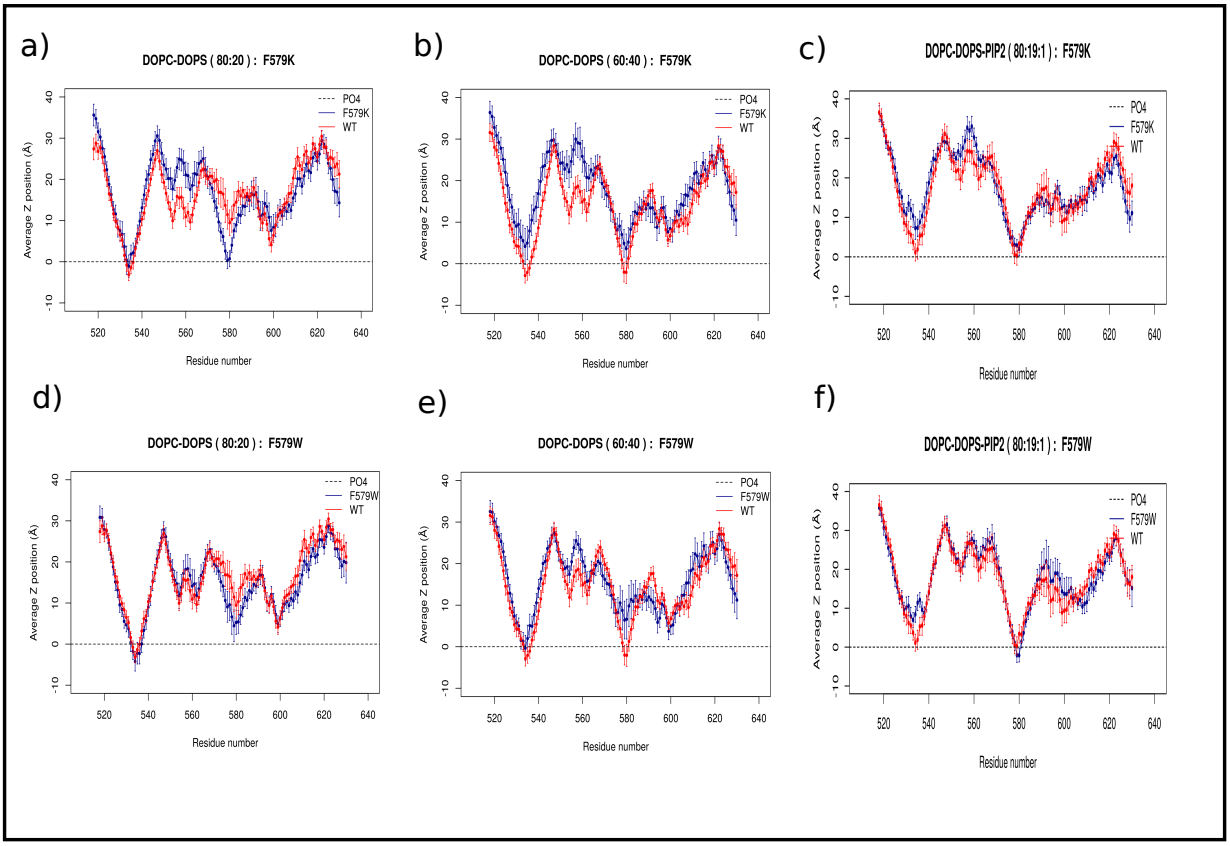

Figure S8: Effect of mutation captured using full atomistic simulation for F579 with different membrane composition and different mutations. The data showing mutation to Alanine is presented in main text. Here, we mutate with Lysine and with Tryptophan to understand if the association is driven by hydrophobic interactions or electrostatic interactions. The different lipid composition chosen are DOPC:DOPS (80:20), DOPC:DOPS (60:40) – highly charged without specificity inducing PIP_2 and DOPC:DOPS:PIP_2 (80:19:1) – canonical composition. The association seems to be due to a complex combination of electrostatic and hydrophobic interactions.

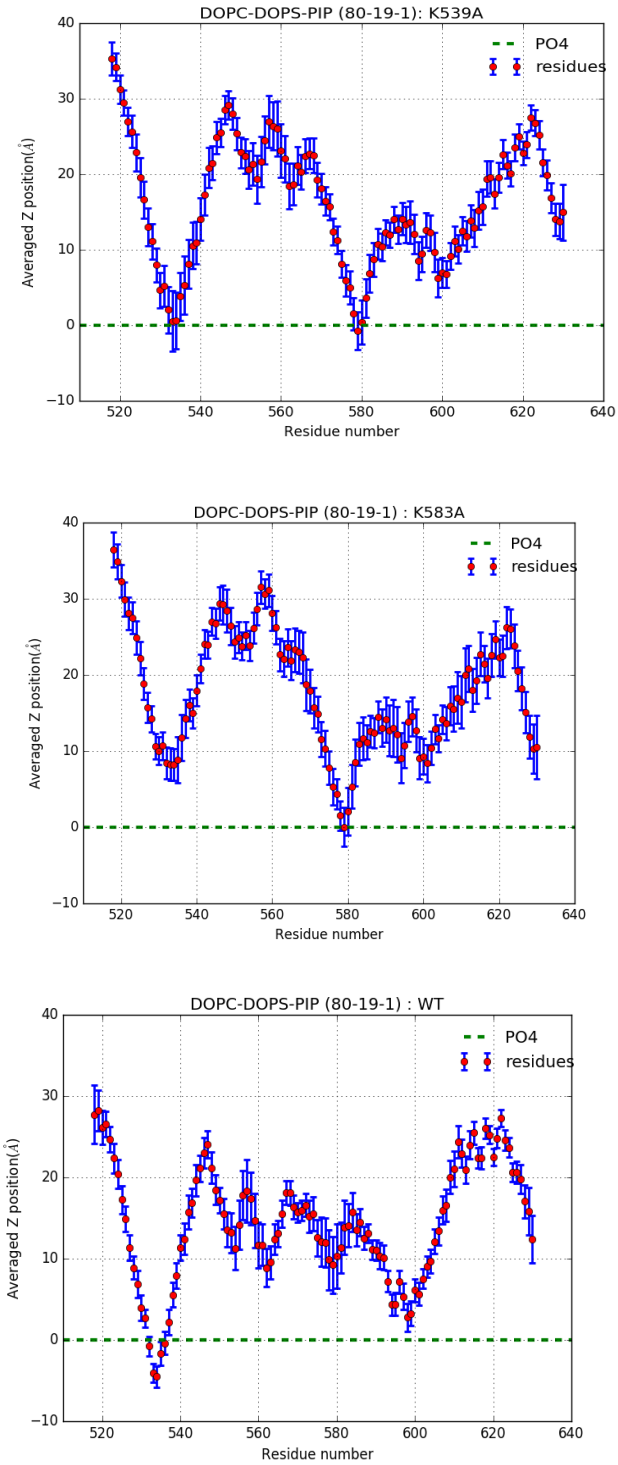

Figure S9: Effect of mutation captured using full atomistic simulation for K539A (top panel) and K583A (middle panel). The WT data is shown in bottom panel for reference. The double mutant data for K539A-K583Ais presented in main text.

1. Plain Metadynamics Simulation Parameters:

(1a) System: Loops-1-3 plain metadynamics

Protein: 1DYN (Pleckstrin homology domain)
Ligand: Inositol triphosphate

Definition of CVs:
CV1: Distance between centre of mass of ligand's inositol ring
and C-alpha atom of residue 600 on loop 3(Tyrosine)
CV2: Torsion angle (A-B-C-D)

A: C-alpha atom of tyrosine-600
B: C-beta atom of tyrosine-600
C: C2 of inositol ring of ITP
D: C5 of inositol ring of ITP

Metadynamics Parameters:
Height of gaussian: 0.5 kJ/mol
Gaussian deposition rate: 1 ps
Length of the simulation: 8.8 ns
sigma of gaussian in CV1 direction:0.05 nm
sigma of gaussian in CV2 direction:0.35 rad
CV1 upper restraint: 1.6 nm with harmonic restraint whose kappa=2000

(1b) System: Loops-1-4 plain metadynamics

Definition of CVs:
CV1: Distance between c.o.m of ligand's inositol ring and C-alpha atom of residue ASP529
CV2: Torsion angle (A-B-C-D)

A: C-beta atom of asparagine-529
B: C-alpha atom of asparagine-529
C: C2 of inositol ring of ITP
D: C5 of inositol ring of ITP

Metadynamics Parameters:
Height of gaussian: 0.5 kJ/mol
Guassian deposition rate: 1 ps
Length of the simulation: 8.8 ns
sigma of gaussian in CV1 direction:0.05 nm
sigma of gaussian in CV2 direction:0.35 rad
CV1 upper restraint: 1.6 nm with harmonic restraint whose kappa=2000

2. Well-Tempered Metadynamics Simulation Parameters:

1a. System: Loops 1-3 Well-Tempered metadynamics

Protein: 1DYN (Pleckstrin homology domain)
Ligand: Inositol triphosphate

Definition of CVs:

CV1: Distance between centre of mass of ligand's inositol ring and C-alpha atom of residue TYR 600 CV2: Torsion angle (A-B-C-D)

A: C-alpha atom of tyrosine-600
B: C-beta atom of tyrosine-600
C: C2 of inositol ring of ITP
D: C5 of inositol ring of ITP

Metadynamics Parameters:

Initial Height of gaussian: 1.0 kJ/mol
Guassian deposition rate: 1 ps

Length of the simulation: 160 ns
sigma of gaussian in CV1 direction:0.05 nm
sigma of gaussian in CV2 direction:0.35 rad

CV1 upper restraint: 1.5 nm with harmonic restraint whose kappa=3000

2b. System: Loops 1-4 Well-Tempered metadynamics

Protein: 1DYN (Pleckstrin homology domain)
Ligand: Inositol triphosphate

Definition of CVs:
CV1: Distance between centre of mass of ligand's inositol ring and C-alpha atom of residue 586 (phenylalanine)
CV2: Torsion angle (A-B-C-D)

A: N atom of phenylalanine 586
B: C-alpha atom of phenylalanine 586
C: C2 of inositol ring of ITP
D: C5 of inositol ring of ITP

Metadynamics Parameters:
Initial Height of gaussian: 1.0 kJ/mol
Guassian deposition rate: 1 ps

Length of the simulation: 110 ns
sigma of gaussian in CV1 direction:0.05 nm
sigma of gaussian in CV2 direction:0.35 rad

CV1 upper restraint: 1.5 nm with harmonic restraint whose kappa=3000

2c. System: Whole Protein Well-Tempered metadynamics

Protein: 1DYN (Pleckstrin homology domain)
Ligand: Inositol triphosphate

Definition of CVs:
CV1: distance between the centroid of protein and the centroid of ligand's inositol ring

CV2: Angle (A-B-C)
A: Centroid of the protein
B: C1 of inositol ring of ITP
C: C4 of inositol ring of ITP

Metadynamics Parameters:
Initial Height of gaussian: 1.0 kJ/mol
Guassian deposition rate: 1 ps

Length of the simulation: 220 ns
sigma of gaussian in CV1 direction:0.05 nm
sigma of gaussian in CV2 direction:0.35 rad

CV1 lower restraint: 1.2 nm with harmonic restraint whose kappa=2000
CV1 upper restraint: 2.8 nm with harmonic restraint whose kappa=2000

3. Justification for using PHD instead of dynamin: It can be argued that the deductions made from simulating the dyn1-PHD on the membrane might be limited in terms of transferability to what could be observed with the full dynamin structure. Though there would be changes, the choice can be justified by looking at some of the experimental work with PHD-mutant or knockouts. In Dar *et al* (1), PHD was replaced by a six residues long His-tag, which affects the fission rate but did not alter any other mechanism of dynamin. Dynamin formed a helix in a similar fashion as it does with WT-PHD. Though tightly coupled to each other, each domain of dynamin has a specific job assigned to it as is the case with most of the multi-domain proteins. Moreover, the sheer size of dynamin makes the computational work prohibitive, even with the largest of computational resource.

4. Effect on bending modulus of membrane due to peripheral protein: Recent article by Fowler *et al* (2) suggests that the contribution of peripheral protein in generating thermal undulation may not be significant enough to affect the bending modulus. The deductions were mostly based on simulations using a small protein tN-Ras. Our results turn out in contrast to the arguments made by the article. Our results show that the shallow-docking peripheral PHDs lower the bending modulus and here could be a couple of possible reasons that could explain this contradiction including the absence of cholesterol which is known to act as a knob to maintain packing "homeostasis" in the membrane. Another crucial factor that supports PHD association is the presence of PIP_2 in our lipid compositions. We observed in our CG simulations (with no PIP_2 molecule in their lipidome), that the PHDs don't stay close to the bilayer for the entire time and some of them actually diffuse long way from headgroup surface. Such behavior was not observed when PIP_2 was added to the system due to the specific binding that occurs between PHD and PIP_2. The other reason could be could be the nature of the protein itself. We would also like to discuss the reduction in bending modulus data in light of several recent studies where different kind of changes in membrane rigidity is observed due to peptides, peripheral and intrinsic proteins. There are several studies where peptides are shown to soften the membrane (3-6) and some very interesting recent work where certain peptides (GWALP in this case) could lead to a liquid-disordered system to have a higher rigidity than ordered systems (7).

5. Effect of lipid composition:

80:20 (DOPC-DOPS): Z-distance analysis of WT-PHD suggest that residues of VL1 are mainly responsible for membrane association. The importance of VL1 is also pronounced in Z-distance analysis of PHD F579 mutants. Interestingly, VL4 association becomes favorable upon the mutations (refer Fig. S8). However, noticeable effects can only be seen in the case of F579A, which suggests firmly that VL4 establishes the contacts with membrane upon this mutation. This behavior can be associated with the small size of alanine. This mutation in VL1 makes it identical to VL4 in terms of hydrophobic residues.

60:40 (DOPC-DOPS): Z-distance analysis of WT-PHD suggest that both VL1 and VL4 loops participate in membrane association. Interestingly, mutations at site F579 seem to have serious impact on membrane binding. Again, this impact is most pronounced in the case of F579A mutation while other mutations seem relatively less lethal (refer Fig. S8). This phenomenon is mainly driven by electrostatics since the membrane is extremely rich in negatively charged PS-lipids. Hence, membrane seems to attract more positively charged residues especially in the region from and nearby VL3 loop.

80:19:1 (DOPC-DOPS-PIP2): In this case, Z-distance analysis provided some extremely crucial insights. VL1 and VL4 are almost equally responsible for membrane association in the case of WT-PHD. Mutation at site F579 severely affects the membrane binding ability of VL1 by decreasing the affinity in a region away from the site of mutation. F579W mutation favors the insertion of VL4 loop compared to other F579 mutations probably because of the bulky-aromatic side group that tryptophan contains, which gets stuck inside upon the insertion and acts as a clamp for membrane association.

References:

1. Dar S & Pucadyil TJ (2017) The pleckstrin-homology domain of dynamin is dispensable for membrane constriction and fission. *Molecular biology of the cell* 28(1):152-160.

2. Fowler PW*, et al.* (2016) Membrane stiffness is modified by integral membrane proteins. *Soft Matter* 12(37):7792-7803.

3. Tristram-Nagle S*, et al.* (2010) HIV fusion peptide penetrates, disorders, and softens T-cell membrane mimics. *Journal of molecular biology* 402(1):139-153.

4. Pott T, Gerbeaud C, Barbier N, & Méléard P (2015) Melittin modifies bending elasticity in an unexpected way. *Chemistry and physics of lipids* 185:99-108.

5. Dimova R (2014) Recent developments in the field of bending rigidity measurements on membranes. *Advances in colloid and interface science* 208:225-234.

6. Pabst G, Danner S, Podgornik R, & Katsaras J (2007) Entropy-driven softening of fluid lipid bilayers by alamethicin. *Langmuir* 23(23):11705-11711.

7. Usery RD*, et al.* (2018) Membrane Bending Moduli of Coexisting Liquid Phases Containing Transmembrane Peptide. *Biophysical journal* 114(9):2152-2164.